

METEOROLOGICAL OFFICE

146543

- 6 SEP 1985

LIBRARY

MET O 19 BRANCH MEMORANDUM No. 81

AN IMPROVED TOVS CLOUD CLEARING SCHEME

- PRELIMINARY REPORT

by P.D.WATTS AUG 1985

Meteorological Office Unit (Met.O.19c),  
Robert Hooke Institute for Cooperative Atmospheric Research,  
Clarendon Laboratory, Oxford, OX1 3PU

NOTE

This paper has not been published. Permission to quote from it should be obtained from the Assistant Director (Satellite Meteorology), Meteorological Office, London Road, Bracknell, Berkshire, RG12 2SZ



## 1 Introduction

---

The Met 0 19 Local Area Sounding System (LASS) currently uses a statistical inversion scheme to produce atmospheric temperature and humidity profiles from TOVS (TIROS Operational Vertical Sounder) brightness temperature measurements. The instruments measure radiances but these are converted to equivalent brightness temperatures in the preprocessing. For the inversion it is assumed that the brightness temperatures have been measured from a field of view (FOV) that is free of cloud, i.e. that they are 'clear-column' brightness temperatures. Whilst clouds barely affect microwave radiation (MSU channels 1,2,3,4) they are generally opaque to infrared radiation (HIRS channels 1-19) which provides most of the sounding information (see Smith et al. 1979 for a description of the TOVS channels and Schwalb, 1978, for further information on the TOVS instruments). Consequently, an important part of any TOVS retrieval scheme is at least identifying, and preferably correcting for, such contamination of the HIRS brightness temperatures. In order to determine that a HIRS FOV is cloud-contaminated some ancillary information is required. This information can be realised from various sources: MSU sounding channels, AVHRR (Advanced Very High Resolution Radiometer) brightness temperatures, forecast temperature fields, etc. Such information can be used to estimate 'clear-column' brightness temperatures against which the measured values are compared to detect non-clear conditions. Because the radiance field is reasonably smooth there is further information on the clear-column HIRS brightness temperature from surrounding FOVs.

Currently, in LASS, measured MSU channel 2 (peaking around 700 mb) is used as a 'pseudo-HIRS' clear-column brightness temperature against which to check for cloud and with which, if possible, to correct for the contamination using the  $N^*$  method (Smith, 1968). Once a suitable pair of adjacent FOVs has been found and the  $N^*$  algorithm applied, no further information on the HIRS brightness temperatures is added. In an optimal clear-radiance scheme all available information would be used. Discussion of the various methods of cloud-clearing and the rationale behind this 'optimal' approach can be found in Eyre (1983). Here we shall reiterate some of the points given in this reference and shall describe how such a scheme has been put into practice.

The new scheme consists of two parts. Firstly there is a cloud-clearing section analogous (but not identical) to the current LASS scheme where initial estimates of the HIRS brightness temperature field and its expected error are obtained. A sequential estimator is then applied to combine all available information, weighted according to the expected errors, on the HIRS brightness temperatures at a FOV. In the scheme this consists of initial estimates at the FOV itself and initial estimates at all other FOVs. In principle any information on a HIRS brightness temperature can be included with the sequential estimator provided that the error characteristics of this information are known.

Section 2 of this paper will briefly describe the methods used to arrive at the initial estimates of the clear-column HIRS brightness temperatures and the associated expected errors. Section 3 details the sequential estimator and describes the constraints on some of the parameters involved. Liberal use has been made of appendices so as not to confuse the issue in these sections. Section 4 addresses the problem of correlated error fields and how it has been tackled. Section 5 presents some preliminary results of the scheme and section 6 outlines further



plans. An appendix C is included which describes the programming structure and details, and is primarily intended to stimulate constructive criticism.

## 2 Preliminary estimation of clear column brightness temperatures

---

The new scheme estimates the clear-column HIRS brightness temperature in each channel at every FOV in the pass along with its expected error. There are four basic routes to a set of clear brightness temperatures depending on the degree and type of cloud contamination. The routes and an indication of the method of error analysis for each are described in the following sections.

### 2.1 Clear conditions

---

Detection of cloud is achieved in a similar manner the present LASS system. A linear combination of HIRS brightness temperatures is used to predict MSU-2 (MSU channel 2) brightness temperature - a regression which is based on clear column measurements:

$$\hat{T}_{m2} = a_0 + \sum_j a_j T_j \quad 1.$$

where  $\hat{T}_{m2}$  and  $T_j$  are predicted MSU-2 and measured HIRS channel  $j$  brightness temperatures respectively and  $a_j$  are the regression coefficients. The coefficients are currently generated within Met 0 19 (see Watts, 1984). This regression has a residual rms error,  $\Delta\hat{T}_{m2}$ , which is known and typically 0.6 K (for clear-column HIRS radiances only). If the predicted MSU-2 brightness temperature is found to be smaller than the measured MSU-2 by an amount greater than this residual, the FOV is assumed to contain some cloud. (In practice HIRS longwave and shortwave are treated separately because of the significantly different effects of cloud on radiances in the two regions.) If this is not the case, i.e.  $\hat{T}_{m2}$  and  $T_{m2}$  agree to within  $\Delta\hat{T}_{m2}$ , we can assume, to within the sensitivity of our detection method, that there is no cloud. The initial estimates of HIRS then are simply the measured values. However, the associated error is not simply the intrinsic noise in the HIRS since we are not entirely certain that the FOV is clear. The error estimation proceeds along similar lines to the partly cloudy case and is given in appendix A.

### 2.2 Partly Cloudy conditions

---

If the FOV is found to be cloud contaminated, i.e.  $\hat{T}_{m2}$  is colder than  $T_{m2}$  by more than  $\Delta\hat{T}_{m2}$ , then the  $N^*$  method is attempted using the most suitable adjacent FOV available. 'Most suitable' in this case means that:

- a) the partner has a smaller predicted MSU-2 value, i.e. is more cloudy. If this (or a similar) constraint were not imposed then,



for example, FOV A could be used with B to give clear radiance estimates for A, and then B with A to estimate radiances at B. Whilst this is not unreasonable (the atmospheres in the two FOVs are assumed identical for  $N^*$  purposes) it would mean that the estimates for A and B were not independent which would be undesirable when running the sequential estimator. This constraint is not required in the current LASS scheme because no attempt is made to estimate clear brightness temperatures at every spot. It is the warmer, less cloudy, FOV that is used as the principal spot - the  $N^*$  cleared brightness temperatures will more nearly approximate to the values appropriate to its atmosphere than to the more cloudy one, because the former provides the most information on the clear-column radiance.

- b) The values of  $N^*_s$  and  $N^*_l$  (separate short and longwave channel estimates) are both required to be  $< 0.75$ . High values of  $N^*$  imply similar cloud amounts in both FOVs and therefore little information on the clear radiances (see error analysis in appendix A).
- c) The magnitude of  $|N^*_s - N^*_l|$  is the smallest of all the possible pairs and is less than some limit (e.g. 0.1). Currently, this is the criterion for 'best pair' though there are other possibilities.

The  $N^*$  method can fail for a variety of reasons and should it do so the HIRS brightness temperatures are estimated from MSU as described in section 2.3. Failures occur because:

- a suitable partner cannot be found i.e. a) or b) above is not satisfied,
- the cleared brightness temperatures fail to pass a test designed to detect contamination by solar radiation (see appendix C),
- the limit defined in c) above is exceeded,
- a check of HIRS-8 estimated from MSU (see section 2.3) against the cleared value shows a large discrepancy. The upper value currently allowed for this discrepancy is the HIRS-8 error estimate which is empirically found to eliminate most rogues.

The error associated with a particular  $N^*$  clearance depends on two factors. Firstly there is the noise present in the radiances, both HIRS and MSU. This originates as radiometric noise and errors due to preprocessing, e.g. limb-correction, etc. (see Watts, 1984). Secondly there is the error in predicting MSU-2 from the HIRS channels - the residual error of the regression. How both of these error sources are amplified by the  $N^*$  algorithm is described in appendix A along with a brief description of the  $N^*$  method itself.



## 2.3 Cloudy conditions

---

This section describes the 'last resort' method of obtaining clear HIRS brightness temperatures (if the MSU data are available). It is used if the FOV is too cloudy to be amenable to  $N^*$  but is also the final route taken by any FOVs that fail the alternatives for whatever reason (except where the MSU is missing, see section 2.4).

Each HIRS channel brightness temperature is estimated using a regression on three MSU channels - 2, 3 and 4 (MSU-1 is difficult to use because of uncertainties in the surface emissivity), that is:

$$\hat{T}_j = b^0 + \sum_i b_j^i T_{mi} \quad 2.$$

with an expected or residual error  $\Delta\hat{T}_j$ . Subscript  $j$  indicates the  $j$ th HIRS channel and  $mi$  the  $i$ th MSU channel. This route is analogous to the MSU-only retrieval in the current LASS system since retrieval on HIRS derived in such a way is essentially a retrieval on MSU. However, the sequential estimator used in the latter part of the process is likely to "advect in" information on vertical structure derived from HIRS radiances in surrounding clear or partly cloudy areas. This route may then provide a more effective way of using MSU sounding information.

In the sequential estimator the error estimates are assumed to be unbiased and uncorrelated. With the MSU regression this was found not to be the case - HIRS estimated from MSU is locally biased and so, over many passes, the error characteristics of the regression might be,

$$\begin{aligned} \bar{E}_j &<< \Delta\hat{T}_j, \\ \sigma(E_j) &= \Delta\hat{T}_j \end{aligned}$$

but locally, 
$$\bar{E}_j = \delta_j, \quad \text{where } |\delta_j| \sim \Delta\hat{T}_j$$

$$\sigma(E_j) << \delta_j$$

where  $E_j$  is the brightness temperature error in channel  $j$ , a bar over a variable indicates a mean value and  $\sigma$  is a standard deviation.

Further discussion of this effect and how it has been dealt with can be found in section 4. The errors in the HIRS derived from MSU are taken to be the residual errors in the regression. This residual is due to two causes; some vertical profile structure is detectable with many HIRS channels but not with relatively few MSU channels, and secondly there is noise in the MSU brightness temperatures. The first cause gives rise to the locally constant error discussed above because the atmospheric profile shape is relatively constant over large areas. Because we remove the estimated bias (section 4) the remaining errors in the HIRS are due to MSU noise, the error in our estimated bias and a contribution due to horizontal structure in the field that is within the resolution of the HIRS sounder but not the MSU. Therefore taking the HIRS error to be the regression residual might seem to be overestimating it but there are good reasons for erring on the high side; of the remaining errors the bias error is very likely to be itself biased (because it is heavily filtered) and the noise in the MSU is due in part to limb and surface emissivity



corrections which also may be locally biased. In summary, the errors in HIRS brightness temperatures resulting from the MSU regression route are expected to be significantly less than the regression residual but are likely to be correlated and therefore should be increased for use in the sequential estimator. Taking the regression residual as the error is probably a reasonable approximation.

#### 2.4 MSU missing

---

If the MSU data are missing or corrupt we have lost the ability to detect cloud contamination of the HIRS and the regression route 2.3 is not available. In this case a search is made in the region of the corrupt spot for a successfully cleared FOV (up to five spots away) and the HIRS and MSU for this spot used. The expected error is suitably enhanced to allow for the distance between the two. Failing this, climatological mean values are used with the climatological variance as the expected error. Corrupt or missing MSU data are not a frequent problem.

#### 3 Sequential estimator

---

The estimator used is a simple scalar one whereby all the available estimates of brightness temperature in one channel are combined in the normal minimum variance way:

$$\frac{\hat{T}_m(+)}{\sigma_m^2(+)} = \sum_n \frac{\hat{T}_n(-)}{\sigma_{mn}^2(-)} \quad 3.$$

with,

$$\frac{1}{\sigma_m^2(+)} = \sum_n \frac{1}{\sigma_{mn}^2(-)} \quad 3a.$$

(where the subscript  $j$  denoting the channel has been dropped for clarity). (-) refers to an initial estimate and (+) to a best estimate. The  $\sigma_{mn}^2(-)$  are error variances of initial estimates appropriate to a remote spot  $n$  and  $\sigma_m^2(+)$  the final error variance of the spot  $m$  being estimated. The summation is over all available estimates ( $n=1, N$ ) of  $T_m$ . Notice that in this formulation the final estimate of  $T$  in a channel is independent of any other channels (see Eyre, 1983). In principle the estimation could be extended to all channels simultaneously.

An efficient and simple way of approximating equation 3 is to use a sequential estimator that runs through the pass (both forwards and backwards) using adjacent previously processed best estimates at each FOV in turn. Explicitly, for a FOV positioned at line  $m$ , spot  $n$ , the forward best estimate of  $T$  is obtained by combining its initial estimate with best estimates from the same spot on the previous line ( $m-1, n$ ) and from the



previous spot on the same line (m,n-1):

$$\frac{\hat{T}_{m,n(+)}^F}{\sigma_{m,n(+)}^2} = \frac{\mu \hat{T}_{m,n}(-)}{\sigma_{m,n}^2(-)} + \frac{\lambda \hat{T}_{m-1,n}(+)}{\sigma_{m-1,n}^2(+) + \beta^2} + \frac{\lambda \hat{T}_{m,n-1}(+)}{\sigma_{m,n-1}^2(+) + \beta^2} \quad 4.$$

Parameters  $\mu$ ,  $\lambda$  and  $\beta^2$  determine the weights given to the various sources and are discussed later.

The backward estimate is similarly:

$$\frac{\hat{T}_{m,n(+)}^B}{\sigma_{m,n(+)}^2} = \frac{\mu \hat{T}_{m,n}(-)}{\sigma_{m,n}^2(-)} + \frac{\lambda \hat{T}_{m+1,n}(+)}{\sigma_{m+1,n}^2(+) + \beta^2} + \frac{\lambda \hat{T}_{m,n+1}(+)}{\sigma_{m,n+1}^2(+) + \beta^2} \quad 5.$$

The final best estimate is a combination of the forward and backward estimates:

$$\frac{\hat{T}}{\sigma^2} = \frac{\hat{T}(+)^F}{\sigma^2(+)^F} + \frac{\hat{T}(+)^B}{\sigma^2(+)^B} \quad 6.$$

With error variance;

$$\frac{1}{\sigma^2} = \frac{1}{\sigma^2(+)^F} + \frac{1}{\sigma^2(+)^B} = \frac{2\mu}{\sigma^2(-)} + \sum_k \frac{\lambda}{\sigma_k^2(+) + \beta^2} \quad 7.$$

where the summation over k refers to the four immediately adjacent spots. If scan-lines are processed alternately left-right and then right-left and if forward and backward filters operate on a given line in opposite directions (see appendix D), the combination of forward and backward estimates advects information approximately uniformly from all directions. The degree of this approximation depends on the size of  $\lambda$  and is discussed in appendix B. Figure 1 illustrates the filtering procedure.

The factor  $\mu$  is not unity as might be expected because the two filter process means that the initial estimate at a spot is used twice. Appendix B derives the appropriate value of  $\mu$ .

A measurement of HIRS at spot (m-1,n) is not strictly a measurement of HIRS at spot (m,n) and its error variance, if used as such, should be increased accordingly.  $\beta^2$ , which is channel dependent, is an addition to  $\sigma^2(-)$  which is intended to account for the spatial variation of the field. Because estimates are 'advected' from all sides, first order variations in the field (i.e.  $dT/dx$ , where x is horizontal distance) are cancelled (assuming the  $\sigma^2(+)$ s are roughly equal) and  $\beta^2$  represents typical second order effects ( $d^2T/dx^2$ ). Appendix B describes how estimates of  $\beta^2$  were obtained for this scheme.

The final parameter  $\lambda$  is intended to avoid overuse of data. Notice that a spot on a different scan-line to the one being estimated can provide information via a variety of routes, the weight given to each route being proportional to  $\lambda$  raised to the power of the number of steps required to reach the central spot. The upper limit on  $\lambda$  then, should ensure that the sum of these weights does not exceed unity (in which case remote spots would have more influence than the central spot). A full



analysis of how  $\lambda$  distributes information has not yet been done though empirical studies suggested that a value of 0.4 gives stable results under a number of conditions and this value has been adopted in the current scheme.

A further role of  $\lambda$ , which may prove to be useful, is in dealing with correlated errors.  $N$  estimates of a temperature with correlated errors do not constitute  $N$  independent pieces of information and the weight given to each should be reduced accordingly.  $\lambda$  could be reduced to achieve this where necessary though this is not done currently in the scheme. The worst case of correlated errors - the MSU regression route - has been accounted for in a more satisfactory way (see section 4).

Appendix B gives further discussion on  $\lambda$ .

#### 4 Analysing the bias field

---

It was noted in section 2.4 that errors in predicting HIRS from MSU are highly correlated locally. Straightforward use of the sequential estimator on a field of brightness temperatures including such biased areas will not solve the problem - the resulting field will still be biased and the estimated error field will be unrealistically low. Reducing  $\lambda$  in such areas should correct the error field but not the brightness temperatures. Ideally we would remove the bias error from the temperature before using the sequential estimator, but of course we do not know the error at the required spots. We do know it, though, at any spot that was found clear or was cleared using  $N^*$ , and, because the error field is highly correlated, we can estimate it elsewhere. This estimation is done in exactly the same way as the sequential estimation of the temperature field; the HIRS from MSU estimation is carried out at all spots (except where MSU is corrupt) and at clear or  $N^*$  spots an estimate of the bias  $\hat{B}_j$ , for HIRS channel  $j$ , obtained:

$$\hat{B}_j = \hat{T}_j(\text{MSU}) - \hat{T}_j(-) \quad 8.$$

where  $\hat{T}_j(\text{MSU})$  is the estimate of HIRS channel  $j$  from the MSU channels. Since we expect most of the error in  $\hat{T}_j(\text{MSU})$  to constitute the bias we set the bias error variance,  $\sigma^2_{B_j}$ , equal to the estimated error in the cleared brightness temperature  $\sigma^2_{\hat{T}_j(-)}$ :

$$\sigma^2_{B_j} = \sigma^2_{\hat{T}_j(-)} \quad 9.$$

The result of this exercise is a field of  $B_j$  and  $\sigma_{B_j}$  (where  $\sigma_{B_j}$ , represents an error distribution in  $B_j$  which is expected to be approximately Gaussian with zero mean) at all clear or part-cloudy spots (except where the surface elevation  $> 1000$  m, because here the regression relation becomes inaccurate). Giving all other spots a value  $B_j = 0$ , and a variance of the regression residual would seem reasonable but as the residuals are often less than  $N^*$  errors the tendency is for  $B$  to tend to 0 in large cloudy areas. This is a consequence of the 'local' problem; climatological values (i.e. 0) with residual errors are not unbiased estimates locally. Consequently, for the bias field, we allow, for all practical purposes,  $\sigma_{B_j} \rightarrow \infty$ . (The same should apply to the brightness temperature field and suggests that, when the MSU data are missing (section 2.4), mean values and variances should not be used. The problem here, though, is not so significant as the variances are much larger than surrounding  $N^*$  or clear error variances and generally there are few spots



where the MSU is missing.) The sequential estimator is used on this field to obtain an analysed field of  $B_j$ . Values of  $\beta^2$  and  $\lambda$  (see table B1) were chosen empirically to obtain a smooth field.

This field can now be added to the temperature field where appropriate (i.e. wherever the HIRS estimate was obtained from MSU) and the sequential estimator run on the result. The mechanics of the scheme are a little different (but equivalent in result) in that the forward B is estimated and added as the forward T filter is run and likewise with the backward filter. This is much quicker computationally than keeping the two operations completely separate. Appendix D describes the mechanics of the filters.

## 5 Preliminary results

-----

The results presented in this section are qualitative only, since a thorough error analysis and comparison with current LASS products has yet to be done (section 6). Several passes have been processed using the new scheme and the one used for demonstration here is a daytime NOAA-7 pass on the 10th October 1984. The AVHRR image was available for this pass and while such data are not currently used in the scheme it provides a useful visual check on the behaviour of the cloud-clearing. Figure 2 is the AVHRR channel 2 (visible) image and shows four regions of interest;

- a) The North West corner which is mainly low scattered cumulus (from the IR image) which provides a good test of the cloud detection and the  $N^*$  algorithm.
- b) A frontal system across the centre of the pass with a thick cirrus shield.
- c) A region to the south of b) mainly of thin cirrus and possibly low stratified cloud.
- d) Low cloud and high ground (Norway) in the North East corner.

Figure 3 is a representation of the cleared HIRS radiances by route taken - the key explains the notation - and gives the total number of spots cleared by each route. An instrument calibration sequence can be seen around line 30 and above this the cirrus shield is indicated by '?' - where there is too much cloud for the  $N^*$  technique. Elsewhere a mixture of routes is evident and there is no large contiguous clear region (as expected from the image).

A 1000-500 mb contoured thickness field derived from the clear radiances is given in figure 4 and should be compared to the current LASS product in figure 5. In both cases the inversion of brightness temperatures to obtain temperature and humidity profiles was achieved by statistical regression. Allowing for the occasional erroneous line introduced by the contouring routine (in the LASS version - 546 dam extreme North and South of the pass) the results are similar excepting a slightly warmer South West corner in the new scheme. There is no apparent increase in resolved horizontal detail and this comes as no surprise considering the weight put on MSU (see figure 3) because of the considerable cloud cover. However, it is expected that the field will be



more accurate overall, particularly in the more cloudy areas.

The equivalent of figure 3 for the current LASS product is figure 6 where 'M' = MSU only, 'C' = clear and '\*' = N-star. The totals by route for both processing routes were;

	LASS		NEW SCHEME	
(C)	115	Clear	238	(.)
(*)	145	N-star	364	(*)
(M)	11	MSU only	2502	(RSsE?)
	0	(other)	32	
	---		----	
Total	271		3136	

Comparing the totals in each scheme it can be seen that:

- the relative proportions of '\*' and 'C' are approximately the same for both schemes,
- there are fewer such clearances, proportionately, in the new scheme (clearances are attempted at four times the number of spots attempted in LASS).

Even allowing for the care taken in the new scheme not to use the same pair of spots twice for N-star clearances, this is an indication that LASS is less sensitive to cloud-contamination. The current LASS rogue-detection is based on retrieved temperature profiles rather than on radiances (as in the new scheme), and this may be the cause of LASS 'missing' cloud. That there are too many 'clear' retrievals in the LASS case is evidenced by comparison with the AVHRR (appendix E). The areas concerned ((a) and (c)) are of low cloud and whilst thicknesses (1000-500 mb) seem unaffected the 'missed' cloud causes the retrieved temperature profile to be 1-3 K cold in layers from 700-1000 mb.

Figure 7 illustrates the filtering procedure and its effect on the radiance field. Shown is a cross-section of the pass at line 7 (the approximate position is marked with a line 'x' on figure 2) the upper plot being unfiltered brightness temperature in HIRS channel 8. The route taken to clear each spot is indicated by the symbol and the associated rms error by the vertical line. 'Regressions' have constant errors, 'clear' errors increase slowly towards the edge of the scan and N-star errors range from the 'clear' value upwards. The lower plot shows the same cross-section after application of the sequential estimator. Note the decrease in errors and the much smoother nature of the field. The filtering procedure, as explained elsewhere, advects information from all directions, not only those shown in the figure, and the section between spots 21 and 36 is a demonstration of this effect.

N\* clearances can be seen to have generally higher errors than the regression route and their inclusion in favour of the latter might be questioned. However, because we assume errors in predicted MSU-2 to be independent, and there is good reason for believing them not to be, our N\* error estimate may well be too high (see appendix A). Even if this is not the case we expect the N\* estimates to be reasonably unbiased in which case they provide good information on the MSU-HIRS bias field.



The filtered field includes the HIRS-MSU bias estimate whenever the route was regression. The plots on figure 8 are equivalent to those on figure 7 but are for the bias estimate. The bias estimate is zero for regression routes with infinite errors (that have been omitted from the diagram). Elsewhere the error is the estimated brightness temperature error. The point role of 'inaccurate'  $N^*$  estimates in helping to determine the bias field is evident.

## 6 Future developments

---

The scheme presently appears to operate satisfactorily and gives results that are not obviously in disagreement with the current LASS system. Whilst there are undoubtedly several areas for improvement the most useful course of action at this stage would be development of a quantitative validation scheme. This would allow assessment of any 'improvements' to the scheme to be made. The current LASS validation scheme colocates soundings with the radiosonde network and compares temperature profiles. Since the new scheme is primarily concerned with cloud-clearing it is thought that a validation scheme using radiances would more clearly monitor its performance - the inversion step required to obtain temperatures simply adds complication. A comparison of cloud-cleared HIRS channel 8 with a value obtained from AVHRR (channel 4) would be a convenient and sensitive estimate of the accuracy of the cloud-clearing though necessarily over a relatively small number of passes. Routine validation will probably be along similar lines to the current LASS quality control, and for a fair comparison with LASS, the same radiosondes and FOVs should be used.

Depending on preliminary results of the validation, the next step may be to rewrite the software, to some extent, for operational implementation. This would be largely concerned with data-set specifications and a clearer 'top down' program structure. The final code should also be sufficiently flexible to allow auxiliary data, such as from forecast models or AVHRR, to aid the cloud-clearing. There is also much redundant diagnostic code that should be removed.

One of the unsatisfactory aspects, in principle at least, of the current scheme is the filtering parameter  $\lambda$ . In practice any modifications to its value would have little practical effect, as discussed elsewhere, but a more thorough understanding of its role and behaviour is desirable. This would be particularly important if any extension were made to the sequential estimator, e.g. if it were to become multivariate.

One recognised cause of error in the scheme (and in LASS) is the approximation of  $N^*$  as a function of brightness temperature rather than one of radiance. There are at least two alternative formulations which should be examined.



A more general rogue detection system, than is currently in place, could be incorporated into the scheme (for example after Purser, 1984). Although rogue detection is done in any assimilation into numerical models, the filtering in this scheme makes it imperative to remove bad clearances at an early stage.

The problem of biases in the predicted MSU-2 brightness temperature (appendix E) could, perhaps, be tackled in a manner similar to the HIRS from MSU bias problem (section 4). The solution is not so straightforward here, though, since no direct measurement of the bias is available - it would have to be inferred from the statistics of the field.

The filtering used in the scheme is in danger of removing genuine features, especially those due to coastlines in the window channels, and a variation in  $\lambda$  or  $\beta^2$  to allow for this could be incorporated.

There may well be a move in the near future to avoid the errors introduced by limb-correcting radiances (especially those that are cloud-contaminated). The scheme should then be adapted to operate on non-limb-corrected data.

In the longer term, advances should be made by including auxiliary data such as AVHRR (Lloyd et al., 1985) and possibly forecast fields (particularly surface temperature). The AVHRR could be useful in directly supplying  $N^*$  values for a pair of FOVs or at least to indicate whether  $N^*$  conditions apply.



## References

---

- Eyre J.R,(1983). 'Towards an optimal approach to cloud-clearing'. Met O 19 Branch memorandum No.72
- Lloyd P.E, Barnett J.J, Eyre J.R,(1985). 'Investigations of AVHRR data to improve TOVS retrievals'. Presented at 2nd International TOVS study conference, Igls, Austria, February 1985.
- Purser J,(1984). 'A new approach to the optimal assimilation of meteorological data by iterative Bayesian analysis'. Preprints, 10th Conference on Weather Forecasting and Analysis. Amer.Meteor.Soc., 102-105 (1984).
- Schwalb A,(1978). 'The TIROS-N/NOAA A-G satellite series'. NOAA Tech. Mem. NESS 95.
- Smith W.L,(1968). 'An improved method for calculating tropospheric temperature and moisture from satellite measurements. Mon Wea Rev, 96, 387-396.
- Smith W.L., Woolf H.M., Hayden C.M., Wark D.Q. and McMillin L.M.,(1979). 'The TIROS-N operational vertical sounder'. Bull. Amer. Meteor. Soc., 60, pp.1127-1140.
- Watts P.D,(1984). 'A study of Local area synthetic coefficients for use in the 'LASS' system'. Met O 19 Branch memorandum No.76



## Appendix A

### N\* method, clear FOVs and error estimation

#### a) Partly cloudy

The N\* method of obtaining a clear radiance estimate from an adjacent pair of partly cloudy fields of view is due to Smith (1968). For a description of the assumptions required by the method about the prevailing conditions see the above reference or Eyre (1983). The measured radiances from spots 1 and 2 can be expressed as:

$$\left. \begin{aligned} R^1 &= N^1 R(\text{cloudy}) + (1-N^1) R(\text{clear}) \\ R^2 &= N^2 R(\text{cloudy}) + (1-N^2) R(\text{clear}) \end{aligned} \right\} \quad A1$$

where R(cloudy) and R(clear) are radiances appropriate to clear and completely overcast conditions respectively, and N<sup>1</sup> and N<sup>2</sup> are the effective fractional cloud covers in spots 1 and 2. Equation A1 can be solved for R(clear):

$$R(\text{clear}) = \frac{R^1 - N^* R^2}{1 - N^*} \quad A2$$

where N\* = N<sup>1</sup>/N<sup>2</sup>, or alternatively solved for N\*:

$$N^* = \frac{R(\text{clear}) - R^1}{R(\text{clear}) - R^2}, \quad A3$$

so that N\* can be found if we have an estimate of some clear radiance along with the partly cloudy radiances. Currently, an approximate expression for N\* is used, where for R<sup>1</sup> and R<sup>2</sup> in the above we use predicted MSU-2 brightness temperatures from the linear combination of HIRS and for R(clear) we use the measured MSU-2 temperature:

$$N^* = \frac{T_{m2} - \hat{T}_{m2}^1}{T_{m2} - \hat{T}_{m2}^2} \quad A3a$$

This is done for longwave and shortwave channels independently with the  $\hat{T}_{m2}$  being estimates of MSU-2 using HIRS channels 1-12 and 13-17 for longwave and shortwave respectively. The N\*s can then be used in A2 to determine clear HIRS radiances.

There are four sources of error in the method:

- a) N\* conditions may not apply. This is not tested for explicitly at the moment - all we have is gross quality control on the N\*s and on the resulting 'clear' radiances.
- b) Errors in R<sup>1</sup>, R<sup>2</sup>. These arise from radiometric noise, calibration, limb-correction etc - all the preprocessing factors (see Watts, 1984) - and is basically the "system noise" up to this stage in the data processing.
- c) Error in T<sub>m2</sub>. As b) but for the MSU channel 2.
- d) Error in  $\hat{T}_{m2}$ . This is effectively the residual error in the regression relation.



In the following error analysis source a) is ignored because, apart from being incalculable, gross quality checks should not permit processing of unsuitable  $N^*$  pairs. All sources of error are assumed to be random, with zero mean (for the purposes of the sequential estimator), though this is not strictly true: both c) and the limb correction parts of b) and d) are likely to locally correlated errors.

Given errors of  $\delta T_{m2}$ ,  $\delta \hat{T}_{m2}^1$  and  $\delta \hat{T}_{m2}^2$ , the error in  $N^*$  becomes:

$$\delta N^* = \frac{\partial N^*}{\partial T_{m2}} \delta T_{m2} + \frac{\partial N^*}{\partial \hat{T}_{m2}^1} \delta \hat{T}_{m2}^1 + \frac{\partial N^*}{\partial \hat{T}_{m2}^2} \delta \hat{T}_{m2}^2 \quad A4$$

$$= \frac{[(T_{m2} - \hat{T}_{m2}^2) - (T_{m2} - \hat{T}_{m2}^1)] \delta T_{m2} - \delta \hat{T}_{m2}^1}{(T_{m2} - \hat{T}_{m2}^2)^2} + \frac{(T_{m2} - \hat{T}_{m2}^1) \delta \hat{T}_{m2}^2}{(T_{m2} - \hat{T}_{m2}^2)^2} \quad A5$$

$$= \frac{(\hat{T}_{m2}^1 - \hat{T}_{m2}^2) \delta T_{m2}}{(T_{m2} - \hat{T}_{m2}^2)^2} - \frac{\delta \hat{T}_{m2}^1}{(T_{m2} - \hat{T}_{m2}^2)} + \frac{(T_{m2} - \hat{T}_{m2}^1) \delta \hat{T}_{m2}^2}{(T_{m2} - \hat{T}_{m2}^2)^2} \quad A6$$

$$= \frac{1}{(T_{m2} - \hat{T}_{m2}^2)} [(1 - N^*) \delta T_{m2} - \delta \hat{T}_{m2}^1 + N^* \delta \hat{T}_{m2}^2] \quad A7$$

If the three  $\delta T$  temperature errors are uncorrelated, the mean square error in  $N^*$  will be:

$$\overline{\delta N^{*2}} = \frac{1}{(T_{m2} - \hat{T}_{m2}^2)^2} [(1 - N^*)^2 \overline{\delta T_{m2}^2} + (1 + N^{*2}) \overline{\delta \hat{T}_{m2}^2}] \quad A8$$

where we have taken  $\overline{\delta \hat{T}_{m2}^1}^2 = \overline{\delta \hat{T}_{m2}^2}^2 = \overline{\delta \hat{T}_{m2}}^2$ . It is likely, however, that  $\delta \hat{T}_{m2}^1$  and  $\delta \hat{T}_{m2}^2$  will be correlated so that, because they have different signs in A7, the last term in A8 will then be an overestimate.

Now approximating equation A2,

$$\hat{T}(\text{clear}) = \frac{T^1 - N^* T^2}{1 - N^*} \quad A9$$

(Equation A2 is exact but for the purposes of error analysis A9 is sufficient.)

$$\delta \hat{T}(\text{clear}) = \frac{\partial T(\text{clear})}{\partial T^1} \delta T^1 + \frac{\partial T(\text{clear})}{\partial T^2} \delta T^2 + \frac{\partial T(\text{clear})}{\partial N^*} \delta N^* \quad A10$$

$$= \frac{1}{(1 - N^*)} [\delta T^1 - N^* \delta T^2] + \frac{\delta N^*}{(1 - N^*)^2} [T^1 - N^* T^2 - (1 - N^*) T^2] \quad A11$$

$$= \frac{[\delta T^1 - N^* \delta T^2]}{(1 - N^*)} + \frac{\delta N^*}{(1 - N^*)} [T^1 - T^2] \quad A12$$



With  $\delta T^1, \delta T^2$  and  $\delta N^*$  independent (there should only be low correlations here):

$$\overline{\delta T^2}(\text{clear}) = \frac{\overline{\delta T^1}^2 + N^* \overline{\delta T^2}^2}{(1 - N^*)^2} + \frac{\overline{\delta N^*}^2}{(1 - N^*)^2} [T^1 - T^2]^2 \quad \text{A13}$$

and substituting for  $\delta N^{*2}$ :

$$\overline{\delta \hat{T}}^2(\text{clear}) = \frac{\overline{\delta T^1}^2 + N^* \overline{\delta T^2}^2}{(1-N^*)^2} + \frac{(T^1 - T^2)^2}{(T_{m2} - \hat{T}_{m2})^2} \left\{ \overline{\delta T_{m2}}^2 + \frac{(1+N^{*2}) \overline{\delta \hat{T}_{m2}}^2}{(1-N^*)^2} \right\} \quad \text{A14}$$

Figure A1 illustrates the  $N^*$  method and the effect of the various error sources.

b) Clear

The method of determining whether a spot is 'clear' has been explained in the main text and the error estimate will be treated here.

In addition to the preprocessing errors introduced into all HIRS spots, genuinely clear of cloud or not, there is an element of uncertainty due to the 'clear FOV criterion' used - we can only detect cloud to within limits determined by the accuracy of the predicted and measured MSU-2. An approximate estimate of the error in  $T_j$  can be obtained by taking the  $N^*$  error (from section a) in the limit of  $N^* \rightarrow 0$  (i.e. equation A14):

$$\overline{\delta \hat{T}_j^2} \rightarrow \overline{\delta T_j^2} + \frac{(T_j - T_j^2)^2 [\overline{\delta T_{m2}^2} + \overline{\delta \hat{T}_{m2}^2}] }{(T_{m2} - \hat{T}_{m2})^2} \quad A15$$

Spot 2 here is some imaginary FOV effectively defining the cloud characteristics and can be considered as completely overcast. Also note that spot 1 is approximately clear:

$$\overline{\delta \hat{T}_j^2} = \overline{\delta T_j^2} + \frac{(T_j(\text{clear}) - T_j(\text{cloudy}))^2 [\overline{\delta T_{m2}^2} + \overline{\delta \hat{T}_{m2}^2}]}{(T_{m2} - \hat{T}_{m2}(\text{cloudy}))^2} \quad \text{A16}$$



Note that for channels unaffected by cloud the noise reduces to the first term only (i.e. preprocessing etc).  $T(\text{cloudy})$  and  $T(\text{clear})$  are undetermined but could be values from a nearby contaminated spot (the  $T(\text{cloudy})$ s would be partly cloudy values,  $T(\text{pc})$ s ).

In evaluating the expressions for  $N^*$  and clear errors  $\delta T_{m2}$  and  $\delta \hat{T}_{m2}$  are known and the fractional multiplier of the second term in A14 is readily calculated for each case. The equivalent fractional term for clear cases in A16 (and see A34) can only be a typical value; in the current scheme it has been estimated with data from a single pass. Clear and cloudy spots were identified and the brightness temperatures used as approximate values of  $T(\text{clear})$  and  $T(\text{cloudy})$ . The fraction was calculated from these for each HIRS channel. Table A1 gives the values found.

The quantity  $\overline{\delta T_j^2}$  is essentially the noise we would expect in genuinely clear FOVs and has contributions from radiometric noise and errors in the preprocessing operations. The limb-correction part of the preprocessing we expect to give errors that depend on the spots scan position - proportional to the secant of the scan angle (Watts, 1984). Other contributions (water vapour corrections, radiometric noise etc) we may expect to have effects approximately constant across the scan. To model these noise contributions we take a basic value (given in table A2) and multiply it by a factor to account for the limb-correction. The factors used are given in table A3 and are proportional to  $\sec \theta$ , where  $\theta$  is the scan angle.

$$\overline{\delta T_j^2} = \text{Fac}(\theta)_j \times (\text{basic value})_j$$

The limb-correction is done in seven steps away from nadir (Watts, 1984) and symmetrically across the scan giving 14 factors in all. This approach to modelling the expected error in 'clear' FOVs is only approximate and there is scope for improvement. In summary; equation A14 is evaluated for each  $N^*$  spot whilst A16 for clear cases is estimated once and for all before processing.

It is possible that the above treatment for 'clear' errors gives a misleading result because a) an  $N^*$  correction is not done in these cases and b)  $N^* \neq 0$  exactly. A full treatment is long and has difficulties but is presented here as it confirms that the form of equation A16 is correct.

The 'clear FOV criterion' is that:

$$\text{DIFF} = (T_{m2} - \hat{T}_{m2}) < \Delta \hat{T}_{m2} \quad \text{A17}$$

where  $\Delta \hat{T}_{m2}$  is currently set equal to the residual error of the MSU-2 regression relation. This relation is essentially

$$\hat{T}_{m2} = \sum_j a_j T_j \quad \text{A18}$$

where  $T_j$  are HIRS brightness temperatures which can be expressed (using an approximation to equation A1) in the form,

$$T_j = (1-\delta N)T_j(\text{clear}) + \delta N T_j(\text{cloudy}) + \delta T_j \quad \text{A19}$$

where  $\delta N$  is the fractional cloud amount ( $N \ll 1$  in these cases). Substituting the expression for  $T_j$  from A19 into A18 and using the resulting expression for  $\hat{T}_{m2}$  in A17 we find,



$$\text{DIFF} = T_{m2} - (1-\delta N)[a_j T_j(\text{clear}) - \delta N \sum a_j T_j(\text{cloudy})] \mp \sum a_j \delta T_j \quad \text{A20}$$

$$= T_{m2} - (1-\delta N)[T_{m2} \mp \delta T_{m2} \mp \delta \hat{T}_{m2}] - \delta N \sum a_j T_j(\text{cloudy}) \quad \text{A21}$$

where we have included the last term in  $\delta \hat{T}_{m2}$  as  $\delta N$  is small. Rearranging terms:

$$\text{DIFF} = \delta N[T_{m2} - \sum a_j T_j(\text{cloudy})] \mp (1-\delta N)[\delta T_{m2} \mp \delta \hat{T}_{m2}] \quad \text{A22}$$

$$= \delta N[T_{m2} - \hat{T}_{m2}(\text{cloudy})] \mp (1-\delta N)[\delta T_{m2} \mp \delta \hat{T}_{m2}] \quad \text{A23}$$

The constraint then becomes:

$$\delta N[T_{m2} - \hat{T}_{m2}(\text{cloudy})] \mp (1-\delta N)[\delta T_{m2} \mp \delta \hat{T}_{m2}] < \Delta \hat{T}_{m2} \quad \text{A24}$$

At this point we have to remove the inequality to continue. Suppose that on average a 'clear' FOV may be described as,

$$\delta N[T_{m2} - \hat{T}_{m2}(\text{cloudy})] \mp (1-\delta N)[\delta T_{m2} \mp \delta \hat{T}_{m2}] = \Delta \hat{T}_{m2}/\alpha \quad \text{A25}$$

where the parameter  $\alpha$  certainly lies between 0 and 1 but is not known. Since  $\delta N \ll 1$

$$\delta N[T_{m2} - \hat{T}_{m2}(\text{cloudy})] \mp \delta T_{m2} \mp \delta \hat{T}_{m2} \approx \Delta \hat{T}_{m2}/\alpha \quad \text{A26}$$

or,

$$\delta N \approx [\Delta \hat{T}_{m2}/\alpha \mp \delta \hat{T}_{m2} \mp \delta T_{m2}]/[T_{m2} - \hat{T}_{m2}(\text{cloudy})] \quad \text{A27}$$

In the scheme  $\Delta \hat{T}_{m2}$  is the regression residual error so that  $\Delta \hat{T}_{m2} = |\delta \hat{T}_{m2}|$ . Therefore,

$$\delta N \approx [\Delta \hat{T}_{m2}/\alpha \mp \Delta \hat{T}_{m2} \mp \delta T_{m2}]/[T_{m2} - \hat{T}_{m2}(\text{cloudy})] \quad \text{A28}$$

$\delta N$  then represents the expected fractional cloud amount missed by the detection system in a clear FOV. To see the effect of this on  $T_j$  note that it is the 'partly cloudy' temperature that we are using as the 'clear' value:

$$T_j(\text{pc}) = (1-\delta N)T_j(\text{clear}) + \delta N T_j(\text{cloudy}) \quad \text{A29}$$

With the preprocessing noise and the undetected  $\delta N$ , the error in  $T_j$  becomes

$$\delta T_j(\text{pc}) \approx \partial T_j(\text{pc})/\partial N \cdot \delta N \mp \delta T_j \quad \text{A30}$$

$$\approx [T_j(\text{cloudy}) - T_j(\text{clear})]\delta N \mp \delta T_j \quad \text{A31}$$

Substituting for  $\delta N$ :

$$\delta T_j(\text{pc}) \approx \frac{[T_j(\text{cloudy}) - T_j(\text{clear})][\Delta \hat{T}_{m2}/\alpha \mp \Delta \hat{T}_{m2} \mp \delta T_{m2}] \mp \delta T_j}{[T_{m2} - \hat{T}_{m2}(\text{cloudy})]} \quad \text{A32}$$

Therefore,



$$\overline{\delta T_j^2}(\text{pc}) \approx \frac{[T_j(\text{cloudy}) - T_j(\text{clear})]^2 [\Delta \hat{T}_{m2}^2 / \alpha^2 + \Delta \hat{T}_{m2}^2 + \overline{\delta T_{m2}^2}] + \overline{\delta T_j^2}}{[T_{m2} - \hat{T}_{m2}(\text{cloudy})]^2} \quad \text{A33}$$

$$\approx \frac{[T_j(\text{cloudy}) - T_j(\text{clear})]^2 [(\alpha^2 + 1) / \alpha^2 \Delta \hat{T}_{m2}^2 + \overline{\delta T_{m2}^2}] + \overline{\delta T_j^2}}{[T_{m2} - \hat{T}_{m2}(\text{cloudy})]^2} \quad \text{A34}$$

This is a very similar result to equation A16 with increased weight on the  $\Delta T_{m2}$  term in acknowledgment of the fact that we don't require  $\hat{T}_{m2}$  to be exactly  $T_{m2}$  for a clear FOV. Since  $\Delta \hat{T}_{m2} \leq 0.6$  K and  $\delta T_{m2} \leq 0.5$  K the modification is only important for  $\alpha$  significantly larger than 0.5. However, we might reasonably expect  $\alpha$  to be 0.5 or less so that equation A16 is probably adequate.



## Appendix B

### Filtering parameters $\mu$ , $\beta^2$ and $\lambda$

---

#### a) $\mu$

---

The final error variance  $\sigma^2$  for a spot surrounded by spots  $k$  ( $k=1,4$ ) is given by;

$$\frac{1}{\sigma^2} = \frac{2\mu}{\sigma^2(-)} + \sum_k \frac{\lambda}{\sigma_k^2(+) + \beta^2} \quad B1$$

Consider the case where there is no useful information on the central spot in the surrounding spots, i.e.

$$\sigma_k^2(+) \rightarrow \infty$$

In this case the final error variance at spot  $(m,n)$  should be the initial error variance i.e.  $\sigma^2 + \sigma^2(-)$ . From 7:

$$\frac{2\mu}{\sigma^2(-)} = \frac{1}{\sigma^2(-)} \quad \text{or therefore; } \mu = 0.5 \quad B2$$

The effect of  $\mu$ , then, is to allow for the initial estimate at a spot being used twice in the two-way filter.

#### b) $\beta^2$

---

The term  $\beta^2$  is an addition to a spot's error variance to account for the variation in the field when estimating values at a remote spot. In order to estimate its size, consider the estimation of spot '0', say, from the four adjacent spots. Suppose that there is no information on spot '0' and also no intrinsic error in the adjacent spots so that the error in '0' is due entirely to our estimates being at remote locations. we can expand the brightness temperatures in the adjacent spots about spot '0':

$$\begin{aligned} T^1 &= T^0 + \partial T / \partial x \cdot \Delta x + \partial^2 T / \partial x^2 \cdot \Delta x^2 / 2! + \dots + O(\Delta x^3) \\ T^2 &= T^0 - \partial T / \partial x \cdot \Delta x + \partial^2 T / \partial x^2 \cdot \Delta x^2 / 2! - \dots + O(\Delta x^3) \\ T^3 &= T^0 + \partial T / \partial y \cdot \Delta y + \partial^2 T / \partial y^2 \cdot \Delta y^2 / 2! + \dots + O(\Delta y^3) \\ T^4 &= T^0 - \partial T / \partial y \cdot \Delta y + \partial^2 T / \partial y^2 \cdot \Delta y^2 / 2! - \dots + O(\Delta y^3) \end{aligned} \quad B3$$

All derivatives are evaluated at spot '0'. An estimate  $\hat{T}^0$  follows;

$$\hat{T}^0 = \lambda (T^1 + T^2 + T^3 + T^4) / 4\lambda \quad B4$$

$$= T^0 + \{ \mp 2 [\partial^2 T / \partial x^2] \cdot \Delta x^2 / 2 \mp 2 [\partial^2 T / \partial y^2] \cdot \Delta y^2 / 2 \} / 4 \quad B5$$

$$\text{or } \delta T^0 = \hat{T}^0 - T^0 = \mp 1/2 [\partial^2 T / \partial x^2] \cdot \Delta x^2 / 2 \mp 1/2 [\partial^2 T / \partial y^2] \cdot \Delta y^2 / 2 \quad B6$$



$$\text{and } \delta \hat{T}_0^2 = 1/4 \{ |\partial^2 T / \partial x^2| \cdot \Delta x^2 / 2 \}^2 + 1/4 \{ |\partial^2 T / \partial y^2| \cdot \Delta y^2 / 2 \}^2 \quad B7$$

or therefore we require that;

$$\beta^2 \sim 1/2 \{ |\partial^2 T / \partial z^2| \cdot \Delta z^2 / 2 \}^2 \quad B8$$

(z represents an arbitrary direction.) Terms of higher order than  $\Delta z^2$  (i.e.  $\Delta z^4, \Delta z^6$  etc) can be ignored as the factorials become large (equation B3), and we can usually assume that the fields do not have large amplitudes in high order components.

To arrive at a value for the expression B8 a single pass was taken, filtered with a 'guess'  $\beta^2$  and averaged over 2x2 boxes to reduce undesirable noise still further. This procedure produces realistic brightness temperature fields from which derivatives can be estimated. Then a finite difference form of B8 was used to estimate  $\beta^2$  from the resulting field:

$$\partial T / \partial z \Big|_{z^0} = [T(z^0 + 2\Delta z) - T(z^0)] / 2\Delta z \quad B9$$

$$\partial^2 T / \partial z^2 \Big|_{z^0} = \{ \partial T / \partial z \Big|_{z^0 + 2\Delta z} - \partial T / \partial z \Big|_{z^0} \} / 2\Delta z \quad B10$$

$$= \{ T(z^0 + 4\Delta z) - T(z^0 + 2\Delta z) - T(z^0 + 2\Delta z) + T(z^0) \} / 4\Delta z^2 \quad B11$$

$$= \{ T(z^0 + 4\Delta z) - 2T(z^0 + 2\Delta z) + T(z^0) \} / 4\Delta z^2 \quad B12$$

from B8 and B12 our estimate of  $\beta^2$  is therefore,

$$\begin{aligned} \beta^2 &= 1/2 \{ \partial^2 T / \partial z^2 \cdot \Delta z^2 / 2 \}^2 \\ &= 1/128 \{ T(z^0 + 4\Delta z) - 2T(z^0 + 2\Delta z) + T(z^0) \}^2 \end{aligned} \quad B13$$

This quantity was calculated for all channels at every other spot along a scan line and averaged over the pass. The resulting figures are given in table B1.

c)  $\lambda$   
-----

To see how information at a single spot is spread throughout the field by the filter, suppose we have an initial error field where some central spot '0' has error variance  $\sigma^2(-)_0$  and all others have  $\sigma^2(-) \rightarrow \infty$ . Then, for a single forward filter, the error estimate at '0' will be  $\mu / \sigma^2(-)_0$ . At the following spot, '1', the combined estimates will be.

$$\frac{\mu}{\infty} + \frac{\lambda \mu}{\sigma^2(-)_0} = \frac{\lambda \mu}{\sigma^2(-)_0}$$

and at '2',

$$\frac{\mu}{\infty} + \frac{\lambda \cdot \lambda \mu}{\sigma^2(-)_0} = \frac{\lambda^2 \mu}{\sigma^2(-)_0}$$

In the reverse filter spot '0' is used on itself again but not on any of the others that were estimated in the forward filter. Therefore combining forward and reverse filters the error in spot '0' becomes  $2\mu / \sigma^2(-)_0 = 1 / \sigma^2(-)_0$  since  $\mu = 1/2$ .



This may be regarded as giving full or 'unit' weight to the observation at spot '0'. The fractional weight given to other spots is a function of  $\lambda$ , for example spot '3' will be  $\lambda^3/2$  and '4' will be  $\lambda^4/2$  etc. Notice that on lines other than the spot '0' line numerous terms are present because the filter not only uses the previous spot but also the previous line. The number of powers present proliferates and quickly becomes very large. Figure B1 shows the field of powers of  $\lambda$  up to 4 only. The constraint on  $\lambda$  must ensure that at any spot the sum of the various terms does not exceed unity ( $< 2$  for the terms in the diagram since they have been multiplied by two). Also note that the field is clearly asymmetric - across track the weight simply decreases as  $\lambda^n$ , along track a series of powers is present. Providing  $\lambda$  is reasonably small the higher powers should have little effect. A theoretical summation for a general spot has not been done but numerical calculations have been performed to see how the field of Figure B1 (up to much higher powers) behaves with various  $\lambda$  values. Results are presented in Figure B2 where the weight is plotted across-track, solid line, and along-track, broken line, for various values of  $\lambda$  and up to the power of  $\lambda^{20}$ . Figure B2(1) is for  $\lambda = 0.45$  and the along and across-track cross-sections are similar. Figures B(2), (3), (4), (5) and (6) are for  $\lambda = 0.48, 0.51, 0.53, 0.58$  and  $0.8$  respectively. There is a serious asymmetry by  $\lambda = 0.53$  and by  $\lambda = 0.58$  weights at remote along-track spots are higher than the central spot.

A simple refinement is to cancel the asymmetry by employing different  $\lambda$ s for along and across track filtering. This has been done (empirically deriving the second  $\lambda$ ) in Figure B3 where (1), (3) and (5) are single parameter results with  $\lambda = 0.35, 0.40$  and  $0.55$  respectively and (2), (4) and (6) are the corrected versions with along-track  $\lambda$ s of  $0.30, 0.33$  and  $0.35$ . With this adjustment we can therefore fairly safely use a range of  $\lambda$  values and retain a reasonable field. In any real case the  $\beta^2$  term will damp the effect of the central spot still further.

Apart from ensuring that a remote weight is  $< 1$  (which is guaranteed with the above two- $\lambda$  system and an across-track  $\lambda$  of  $< 1$ )  $\lambda$  should provide the desired filtering strength. The distance, in spots, from the central spot required to reduce the weight to  $1/e$  of the central value for various values of  $\lambda$  are;

$\lambda = 0.3$	distance = 0.42
0.4	0.54
0.5	0.72
0.7	1.40

The value of 0.4 used suggests that we are aiming for a resolution of around 1-2 spots which (with, for example, the  $N^*$  method making adjacent spots dependent) seems a reasonable value to aim for. The current scheme uses a single  $\lambda$  parameter.



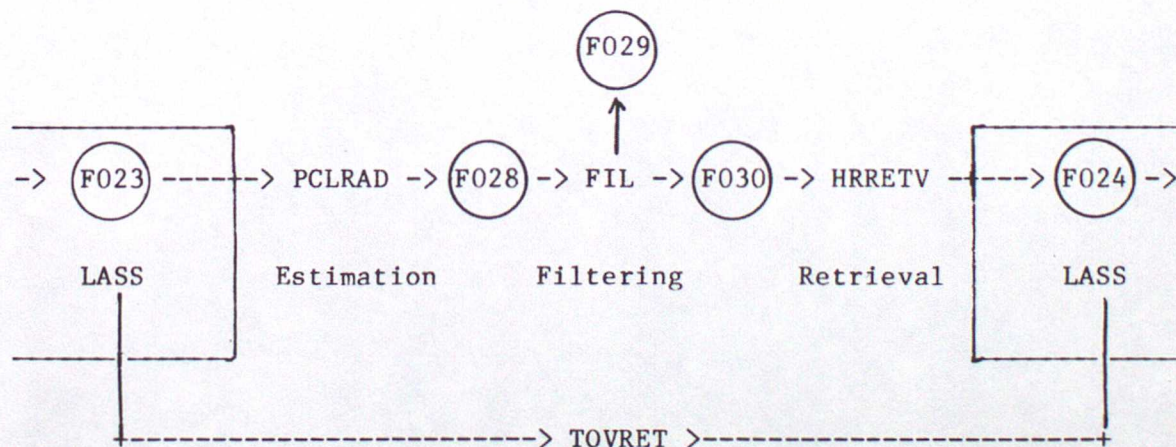
## Appendix C

### Coding structure of the 'Preliminary cloud-clearing' routine - PCLRAD

This appendix is primarily intended to describe how the preliminary clear radiance section of the scheme runs with respect to programming structure and will complement the comments in the code. However, in section C1 the opportunity is taken to describe how the modules of the new scheme, taken as a whole, fit into the existing LASS software. Section C2 describes the mechanics of PCLRAD and finally section C3 lists details for the record.

#### Section C1

The starting point of the cloud-clearing scheme is the 'sounder' file, F023, which contains limb-corrected, calibrated, earth located data produced by TOVPRE in the LASS scheme. PCLRAD, FIL (the filtering routine, described in appendix D) and an inversion module HRRETV (to calculate temperature and humidity profiles from the TOVS brightness temperatures) effectively replace the LASS routine TOVRET. The output file of HRRETV is accordingly in the format of the LASS 'retrieval' file, F024. The intermediate data sets linking the three new modules are the PCL file F028 (the structure of which is documented at the end of this appendix) and the DFL file F030. The structure of the DFL file is identical to the PCL file but contains filtered brightness temperature and error values whereas the PCL file contains the preliminary estimates of the brightness temperatures and their errors. A further file of the same structure, F029, is required to link the forward and reverse parts of the filter but is not retained after the processing is complete. In summary, LASS and the new cloud-clearing modules fit together as follows:



Although the three new modules replace the current LASS scheme's TOVRET as shown above, several 'post-retrieval' operations in LASS become redundant. For example, with the new scheme we have a complete field of HIRS data and therefore a complete field of retrievals (if required). The LASS module ENHRET, which in areas of sparse HIRS data fills in with MSU-only soundings, is no longer required. LASS modules FILRET (filtering bad soundings), REDRET (removing redundant soundings) and COMRET (compressing the retrieval file) could probably all be removed.



## Section C2

PCLRAD runs using a 3-line buffer of the form ( HIRS data etc : scan-spot : line (1,2,3) : error data etc ) dimensioned (36,56,3,2) so that, for example, element (11,3,2,1) will contain HIRS-8 brightness temperature for spot-3 and line 2 (of the three) and (11,3,2,2) will contain its expected error. A similar buffer is held for the bias estimates dimensioned (19,56,2,2). We have a three line structure because the  $N^*$ -method uses 3x3 boxes. Given a current 3-line buffer the processing proceeds as follows:-

- a) Check through line (3) for possible clear radiances and store the differences found between the predicted MSU-2 and the measured value. Flag those FOVs that are found to be clear. If this is not done at this stage we will be carrying out the MSU-2 regression (on line 3 spots) up to three times more often than necessary in the  $N^*$  run (c).
- b) Save the centre line (2) for  $N^*$  in the next cycle.
- c) Run through central line (2), using  $N^*$  wherever possible. If  $N^*$  fails use regression on MSU.
- d) Output central line (2) (temperatures and biases)

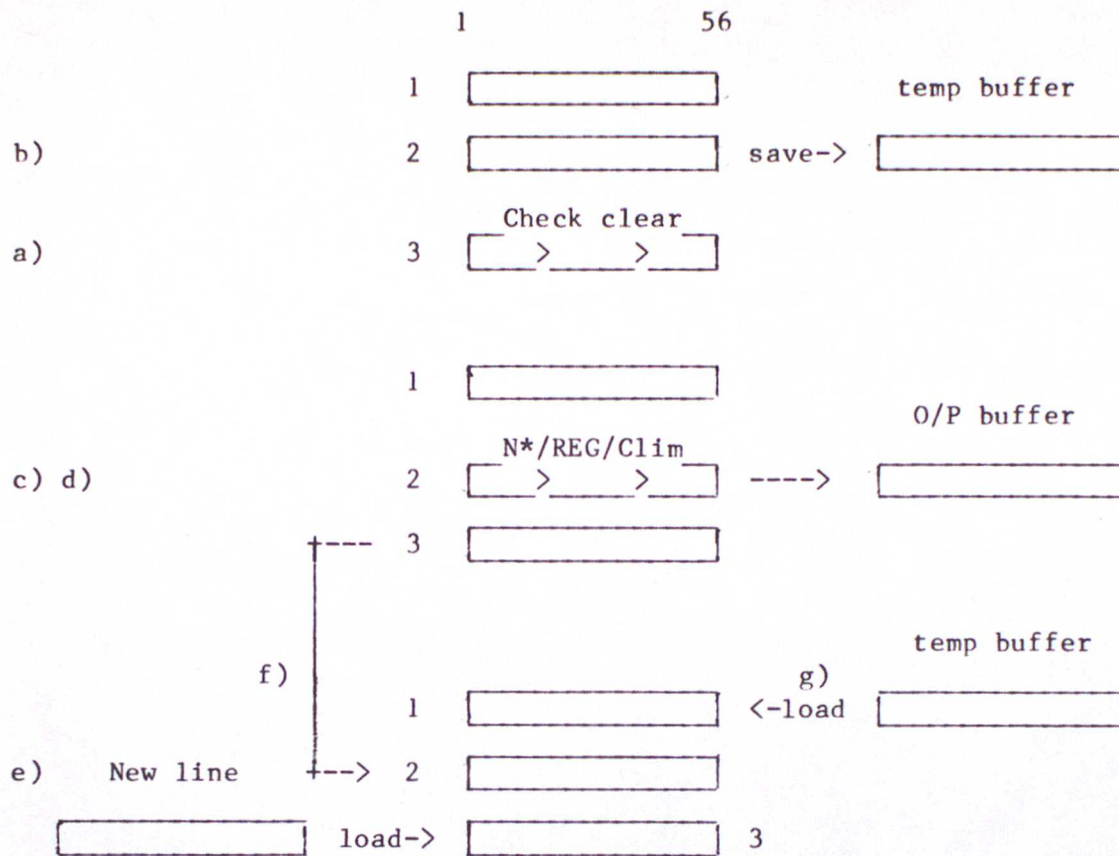
To increment the current line;

- e) Copy old slot-3 to slot-2
- f) Obtain new line (using subroutine LINGET) and put it into slot-3 of buffer.
- g) Copy saved slot-2 to slot-1

The whole cycle is shown diagrammatically in figure C1. Slightly different procedures apply if slot-2 is the first or last lines in the pass since then slot-1 or slot-3 respectively is not available.



Figure C1



### Section C3

Some details, not made clear in the main text, are now given for the steps a), c) and e).

#### a) Check for clear.

1) Get surface elevation (using routine LANSEA).

2) Check MSU data. If any MSU channel brightness temperature is outside the limits 170-320 K a search is made of nearby spots - up to 5 distant for good ( $N^*$  or clear) HIRS and MSU data (subroutine MSUCLIM). On the current line (3) and on the previous line (2) only 'clear' spots can be found because the  $N^*$  processing has not yet covered these lines. Ahead of the current spot on line (3) there is no cleared data but on line (1) both clear and  $N^*$  may be found. Failing this search, climatological mean values are used with climatological variances as the error variances.

3) Check that no HIRS brightness temperatures are  $> 500$  K. If this fails estimates of HIRS are obtained by regression on the MSU (subroutine HIRSREG). HIRS error variances are taken to be the residual errors of the regression.

4) Check predicted MSU-2 against the measured value for possible clear



radiances. If differences (long and shortwave) are both less than their respective residual errors then check for solar contamination (subroutine SOLREF). This latter check is the same as the current LASS system check -  $\text{HIRS}(19) - \text{HIRS}(18) < 10 \text{ K}$ , and  $\text{HIRS}(18) - \text{HIRS}(8) < 20 \text{ K}$ . If the spot fails then it is flagged.

- 5) If, after all, the spot is clear, it is flagged appropriately and the HIRS errors are calculated according to sappendix A. A regression estimate of the HIRS channels is made (HIRSREG) so that a value of the bias (in the regression route) can be obtained by comparison with the measured brightness temperatures. (This is done by subroutine STATS which currently also carries out diagnostic calculations). The bias estimate is used if the elevation is less than 1000m.

c)  $N^*$  on centre line

- 1) Loop over spots 1-56 for slot-2 (centre line). If a spot is flagged clear move to next spot. If a spot is flagged contaminated by solar radiation then obtain HIRS by regression on MSU.
- 2) Get available spots for  $N^*$ . The 3x3 box is designated as follows:

9	8	7	1
6	5	4	2
3	2	1	3
IELE-1 IELE IELE+1			

All spots are searched for a possible  $N^*$  pair with spot 5. This is done by looping  $I = \text{MINI}, \text{MAXI}$ ;  $J = \text{MINJ}, \text{MAXJ}$ ; I being the spot number and J the line number in the 3-line buffer. Normally;

MINJ = 1                      MAXJ = 3  
 MINI = IELE-1              MAXI = IELE+1

the exceptions being,

First line of pass : MINJ = 2  
 Last line of pass : MAXJ = 2  
 First spot of scan : MINI = IELE  
 Last spot of scan : MAXI = IELE

The spot number, given in the above boxes, is derived from  $II = \text{IELE} - I + 11 - 3 \times J$ . Adjacent spots are searched by looping from  $II = 1, 9$  and if a spot is not flagged already cleared its MSU and HIRS temperatures are loaded into the IIth slot of a 9-slot buffer.

- 3) This gives us all the possible  $N^*$  pairs for use with spot 5. The







```
MLIN+1 !                last LINE record                !
-----
MLIN+2 !                SUMMARY record                    !
```

HEADER RECORD.                      Record 1 in the data set.

WORD

1,1,1	Start date Year*1000 + Month*100 + Day
2,1,1	Start time. Hours*1000 + Mins*100 + Sec
3,1,1	(End time.)
4,1,1	Number of HIRS lines.
5,1,1	Satellite ID. 1 or 2
6,1,1	(Process status )
7,1,1	Node (+1 Northbound, 2 Southbound)
8,1,1	N* pair (0=>smallest ns-nl : 1=>nearest 0.5)
9,1,1	MSU coefficients (1=NESDIS , 2=LASC)
10,	
11,	†
36,56,2	† not used

DATA RECORDS.

Records 2 - 151 (MAX)

Each valid data record contains data from one line.

### FORMAT OF DATA

WORD

1,ispot,1	Latitude *100	1,ispot,2	TYPE CLEAR
2,ispot,1	Longitude *100	,2	not used
3,ispot,1	Solar zenith angle * 100	,2	not used
4,ispot,1	Channel 1 temperature * 100	,2	error
5,ispot,1	Channel 2 temperature * 100	,2	error
6,ispot,1	Channel 3 temperature * 100	,2	error
7,ispot,1	Channel 4 temperature * 100	,2	error
8,ispot,1	Channel 5 temperature * 100	,2	error
9,ispot,1	Channel 6 temperature * 100	,2	error
10,ispot,1	Channel 7 temperature * 100	,2	error
11,ispot,1	Channel 8 temperature * 100	,2	error
12,ispot,1	Channel 9 temperature * 100	,2	error
13,ispot,1	Channel 10 temperature * 100	,2	error
14,ispot,1	Channel 11 temperature * 100	,2	error
15,ispot,1	Channel 12 temperature * 100	,2	error
16,ispot,1	Channel 13 temperature * 100	,2	error
17,ispot,1	Channel 14 temperature * 100	,2	error
18,ispot,1	Channel 15 temperature * 100	,2	error
19,ispot,1	Channel 16 temperature * 100	,2	error
20,ispot,1	Channel 17 temperature * 100	,2	error
21,ispot,1	Channel 18 temperature * 100	,2	error
22,ispot,1	Channel 19 temperature * 100	,2	error
23,ispot,1	MSU channel '5' bright tem. * 100	,2	not used
24,ispot,1	MSU channel 1 bright tem. * 100	,2	error
25,ispot,1	MSU channel 2 bright tem. * 100	,2	error



26,ispot,1	MSU channel 3 bright tem. * 100	,2	error
27,ispot,1	MSU channel 4 bright tem. * 100	,2	error
28,ispot,1	View zenith angle *100	,2	not used
29,ispot,1	Finished process indicator (1)	,2	not used
30,ispot,1	MSU-2 <sup>©</sup> Long 'OPER'	,2	" 'NOOP' (36)
31,ispot,1	MSU-2 <sup>©</sup> Short 'OPER'	,2	" 'NOOP' (37)
32,ispot,1	DIFF Long 'OPER'	,2	" 'NOOP' (38)
33,ispot,1	DIFF Short 'OPER'	,2	" 'NOOP' (39)
34,ispot,1	MSU-2 <sup>©</sup> Long 'cleared' 'OPER'	,2	" 'NOOP' (40)
35,ispot,1	MSU-2 <sup>©</sup> Short 'cleared' 'OPER'	,2	" 'NOOP' (41)
36,ispot,1	not used	,2	not used

NOTE 1: TYPE CLEAR is the route indicator:

100 = Climatology  
 200 = " (neighbour search)  
 300 = N\* method  
 400 = Clear

Regression because:

500 = HIRS missing  
 600 = Solar contamination Pre-N\*  
 700 = N\*s-N\*1 too large  
 800 = Solar contamination Post-N\*  
 900 = N\* result out of error range with regression  
 1000 = N\* fails - no suitable adjacent spot

NOTE 2: MSU-2<sup>©</sup> refers to a predicted MSU channel 2 brightness temperature eg. from HIRS longwave. 'DIFF' is the difference between the measured MSU-2 and a predicted value.

NOTE 3: OPER and NOOP refer to the type of regression coefficients used - two sets run in parallel at the moment, the set in slot-1 are 'operational' Those in slot-2 are used for comparison. They can be switched with a data card.

NOTE 4: MSU channel '5' is an MSU channel 1 brightness temperature not corrected for surface emissivity etc.



## Appendix D

### Coding structure of FIL

The module FIL does forward, backward and combined estimation of the brightness temperature field in the manner of the sequential estimator described in the main text. The forward filter (FF) takes input line data from F028, the output of PCLRAD, and writes to an intermediate set F029. The backward filter (BF) reads from F028 and from F029 and writes to F030.

Two 2-line buffers are used, one for the 36 HIRS/MSU data etc, (36,56,2,2), and one for the bias estimates, (19,56,2,2). We have a two line structure here because the filters use the previous spot on the same line and the same spot on the previous line in the estimate. With a new two line buffer the procedure is:

- a) Decide which way to step through line 2 of buffer. This alternates each line and FF and BF work in opposite directions. Thus, if;

modulo (line number,2)	= 1	FF steps +ve	2,56
		BF steps -ve	55,1
modulo (line number,2)	= 0	FF steps -ve	55,1
		BF steps +ve	2,56

- b) Run filter in appropriate direction. At each spot the bias estimate is done first so that it can be added to the temperature estimates before they are filtered. A missing bias estimate (there will normally be many) is given an error variance of the regression residual (which may be expected to be the 'climatological variance' of the bias) multiplied by 100. This approximates to a value  $\sigma^2 \rightarrow \infty$ .
- c) Once the bias estimates are available the brightness temperatures are estimated. The bias is added to T only if a regression route was used. It is not added to channels 1-3 and 17 unless the cause of the regression route was 'HIRS missing'. This is because these channels peak high enough in the atmosphere not to be contaminated by cloud and so, unless the HIRS data are missing altogether, channels 1, 3 and 17 are always 'clear'.

- d) Finish line, output to F029.

To increment line;

- e) Copy line 2 to line 1 of buffer.

- f) Read new line of data from F028 (starting line 2 ending last line of pass). Load into line 2 of buffer.

The backwards filter runs as above but includes the final combination of FF and BF estimates. In addition to a), b) and c) above;

- c2) Combine FF and BF estimates of bias (only required for diagnostics)
- c3) Combine FF and BF estimates of temperature and error.



c4) Finish line, output to F030.

And to increment line;

a) Copy line 2 to line 1.

b) Read new line of data from F028 (starting last but one line of pass ending line 1).

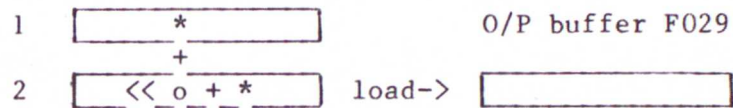
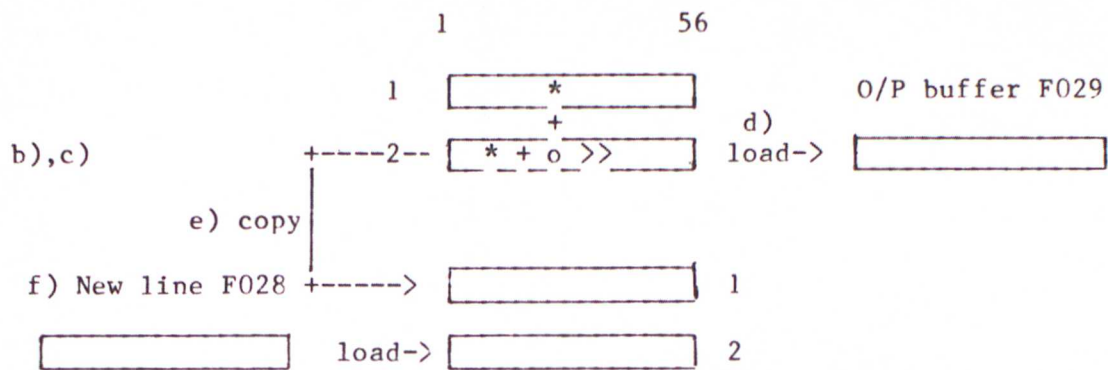
c) Read new line of FF data from F029

The whole filtering procedure is shown diagrammatically in figure D1.

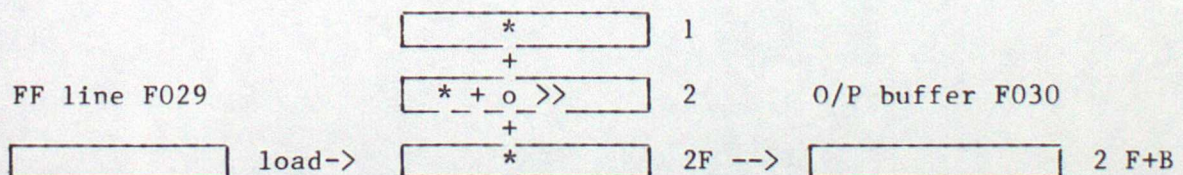
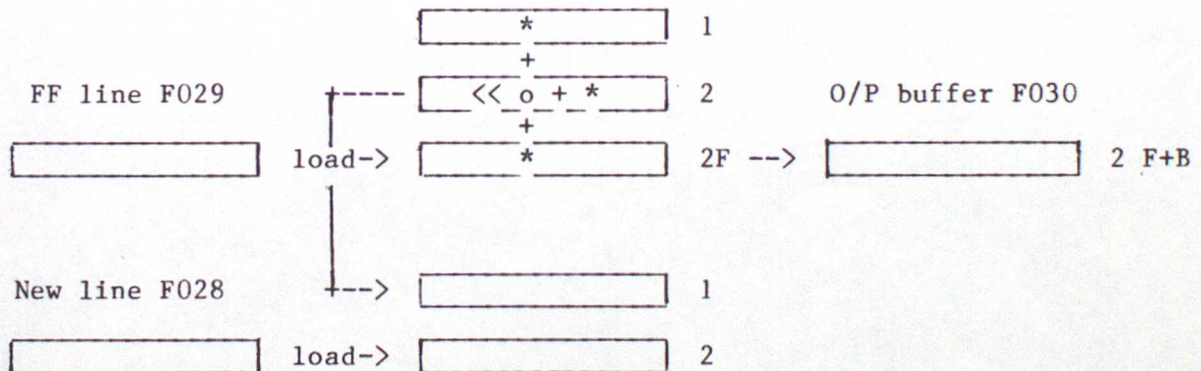


Figure D1

Forward filter



Backward filter



Where throughout 'o' refers to the spot being estimated, '\*' to spots, already processed, being used in the estimation and  $\gg$  to the direction of the filter.



## Appendix E

### Case study on LASC and NESDIS MSU-2 coefficients

This appendix describes the case study undertaken in the main text (NOAA-7, 12th Oct. 1984) but with the emphasis on the behaviour of the cloud-clearing mechanism.

In addition, a comparison is made between results obtained using two different sets of regression coefficients. These sets are: the archived LASS coefficients for the appropriate date (these are received on a regular basis from NOAA/NESDIS) and a set generated 'in house' from archived local area sondes. The latter, LASC (local area synthetic coefficients), are described in Watts, 1984. The cloud-clearing scheme currently allows the two sets of regression coefficients to be used in parallel, one, the 'Non-Operational' set, doing 'dummy' cloud-clearing. Both sets of coefficients are applied to their respective 'cleared' radiances to give a 'cleared' MSU-2 which, ideally, should be within the regression residual of the measured value. If it is not, then the cloud-clearing probably has not worked. Whether this is a good rogue detector has not been investigated. The 'Operational' coefficients used in this case were the appropriate LASC set and an archived NESDIS set (for day 289, 1984) provided the dummy run.

The current LASS system produces a file of the 'sounder' data (calibrated, located and limb-corrected) ordered channel by channel rather than by FOV. This file, F022, is designed to be used for image displays and a similar 'image' file is produced at the end of the new cloud-clearing scheme. It, however, contains all the information in F028 and additionally retrieved temperature and humidity data from F024 (see appendix C). This file can be displayed in conventional manner (i.e. as an image) or can be used in conjunction with a routine which colocates HIRS and AVHRR to within one or two kilometres. An outline of the HIRS footprint and the value of any of the parameters in the 'image' file is displayed at each HIRS location, overlaid on the AVHRR image (see figure E1). This technique is particularly useful for investigating the behaviour of the MSU-2 prediction and therefore the  $N^*$  method.

The results of a run with the NESDIS coefficients in 'operational' role have not been presented in detail but such a run produced fewer 'clear' spots and also less  $N^*$  successes. The principle reason seems to be that MSU-2 predicted from NESDIS coefficients,  $T_{m2}(N)$ , is biased cold and obviously clear spots were judged cloudy. A smaller bias of opposite sign was found with the LASC version,  $T_{m2}(L)$ , giving 'clear' where there was some cloud contamination. (This general discussion refers to the longwave  $T_{m2}$  - the shortwave prediction was studied less but appeared to be less biased generally for both types of coefficients).

Various regions of the pass are now described in a little more detail, particularly the North West corner for which copies of the image display are given. Figures E1 to E4 show the displays available, giving the HIRS footprints overlaid on the AVHRR channel 2 (visible) image. The symbol in the centre of the footprint is the route indicator as in figure 3 and the number above is the quantity  $(T_{m2} - \hat{T}_{m2}) \times 10$ . A negative value of this quantity therefore indicates that the regression produced an MSU-2 temperature greater than that measured. The whole AVHRR channel 2 image is given in figure 2.



- a) The North West corner contains a sharp cirrus edge and low level, well defined cumulus. Figure E1 is a display of the difference between the longwave  $\hat{T}_{m2}(L)$  and the measured MSU-2 for this region and shows the predicted value to be biased by approximately +0.3 K so that low cloud covering up to 4/10 of an FOV is missed. The effect of this low cloud on HIRS channel 7 is  $\sim 1.0$ - $1.5$  K and this causes the retrieved temperature profiles to be cold by about 2.0 K in low layers. The  $\hat{T}_{m2}(N)$  are biased  $\sim -1.0$  K giving very few FOVs judged clear (Figure E2). (Note that the centred symbols still refer to the LASC processing route.) The LASC shortwave, figure E3, shows no real bias but the NESDIS shortwave, figure E4, is consistently cold by  $\sim 0.5$  K. Other points arising from figure E1 are the large change ( $\sim 2.0$  K) between clear and totally cloudy FOVs and the significant number of apparently good  $N^*$  candidates that failed for some reason or other. Comparing all the figures it can be seen that the NESDIS coefficients are much less sensitive to the low cloud. (It should be noted that the lightening of the sea surface towards the left of figures E1-4 is due to sun-glint and such an effect is not present in the infra-red image.)
- b) In the South West corner there are no well-defined clear areas but  $\hat{T}_{m2}(L)$  appears to have a bias of 0.5-1.0 K.  $\hat{T}_{m2}(N)$  is not biased but is variable in apparently clear areas. The LASC coefficients detect the thin cirrus but because of the bias pass the spots as clear - the effect on HIRS channel 7 being about 1.0 K. A section of low cloud, missed by NESDIS, is only partially detected by LASC, again because of the bias. Here HIRS channel 7 is affected by  $\sim 3.0$  K.
- c) The North East corner, around Denmark and Norway, is reasonably cloud-free.  $\hat{T}_{m2}(L)$  has its usual positive bias which changes rapidly towards the edge of the scan (from 0.5  $\rightarrow$  1.1 K in 3 or 4 FOVs).  $\hat{T}_{m2}(N)$  is biased  $\sim -1.6$  K. The effect of the high terrain on LASC is very apparent - from the Barents Sea to the mountains of Norway  $\hat{T}_{m2}(L)$  changes by  $\sim 2.5$  K. With  $\hat{T}_{m2}(N)$  the effect is small (0.3K) and variable.

In summary, the LASC MSU coefficients have a greater sensitivity to small amounts of cloud contamination (whether low cloud or thin high cloud) than the NESDIS coefficients. This may be expected as LASC are generated from good 'clear' (i.e. synthetic) radiances whereas NESDIS have to rely on noisy cloud-cleared real radiances. However, this sensitivity is often swamped by local biases, representing the residual error in the regression relation, which often causes significant cloud cover to be missed altogether and presumably lowers the accuracy of any  $N^*$  clearance. An analysis of these biases, as in the HIRS from MSU case, would be desirable but would be difficult to achieve because, other than comparison with AVHRR data that is not generally available at this time, we have no direct measure of it.

Figures E5a-d are scatter plots for the whole pass and whilst illustrating some of the points made above also provide a quick-look 'debugging' guide in case the cloud-clearing fails to work as expected. The plots show measured MSU-2 against the four predicted versions (long and shortwave from 'Oper' -LASC, and 'Non-oper' -NESDIS coefficients). The general scatter indicates clearly a cloudy set of FOVs ( $\hat{T}_{m2} \ll T_{m2}$ ) and a more or less well defined band of 'clear' FOVs (which contain some of the areas of low-cloud). Figures a) and b) show the 'clear' band less



well defined (and also colder cloudy  $\hat{T}_{m2}$ s present) in LASC longwave than in NESDIS. The line of the 'clear band' is nearer 45deg in LASC; NESDIS coefficients gave  $T_{m2}$  biased cold in cold regions and biased warm in warm regions. In all plots the cold 'toe' just displaced from the axis is a region of low cloud. High ground over Norway has much the same effect but is a little warmer.

Finally, figures E6a-d compare longwave with shortwave estimates of MSU-2 (a and b) and NESDIS with LASC (c and d). From a and b we see that LASC shortwave estimates in cloudy regions differs from the longwave estimate more substantially than with NESDIS coefficients. Also the agreement between the two estimates in clear regions is rather better with the LASC coefficients. Ec and d show that the two sets of coefficients predict similar  $\hat{T}_{m2}$ s from the shortwave HIRS channels but markedly different ones from the longwave channels.

It should be stressed that the results and conclusions presented in this appendix are derived from examination of a single pass and may not be generally valid.



Table A1 Fractions used in the clear error estimation

HIRS ch	Fraction	HIRS ch	Fraction
1	0.00	11	1.50
2	0.00	12	0.35
3	0.00	13	3.00
4	0.17	14	2.30
5	0.75	15	1.00
6	1.40	16	0.01
7	2.00	17	0.00
8	3.00	18	5.00
9	1.20	19	3.00
10	2.70		

Table A2 Noise assumed in genuinely clear nadir FOVs

HIRS - 1,19 = 0.4K, MSU - 1,4 = 0.5K

Table A3 Factors to account for limb-correcting errors

Scan position from nadir	1	5	9	13	17	21	25
Factor	: 0.917	0.930	0.954	1.00	1.06	1.16	1.30

Table B1 Filtering parameters  $\beta^2$  and  $\lambda$

$\beta^2$ :

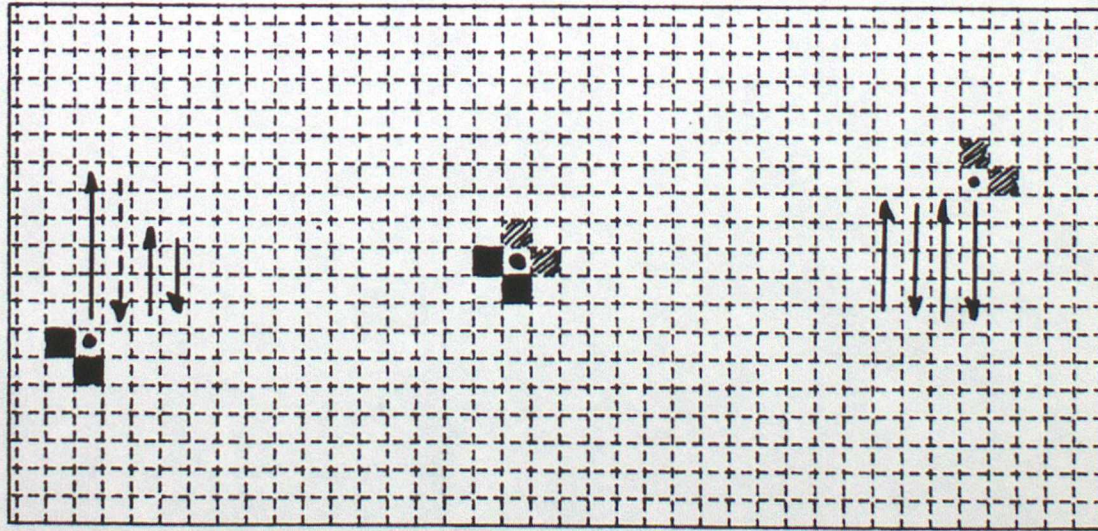
Channel	Temp	Bias	Channel	Temp	Bias
H-1	0.03	0.03	H-12	0.15	0.15
H-2	0.00	0.00	H-13	0.22	0.22
H-3	0.00	0.00	H-14	0.08	0.08
H-4	0.01	0.01	H-15	0.02	0.02
H-5	0.02	0.02	H-16	0.01	0.01
H-6	0.04	0.04	H-17	0.01	0.01
H-7	0.12	0.12	H-18	0.49	0.49
H-8	0.37	0.37	H-19	0.54	0.54
H-9	0.63	0.63	M-1	0.01	0.01
H-10	0.29	0.29	M-2	0.01	0.01
H-11	0.15	0.15	M-3	0.01	0.01
			M-4	0.01	0.01

$\lambda$  (Temp) = 0.40       $\lambda$  (Bias) = 0.48



# Figure 1 Forward and Reverse filters

LINE ~ 150



LINE = 1

SPOT 56

SPOT 1

SINGLE  
PASS

The solid squares in the top left of the pass are the spots used in the 'forward' estimation of the adjacent dotted spot. The cross-hatched squares, bottom right, are those used in the 'backward' estimation of a second dotted spot. The squares in the centre are intended to show the symmetrical result of both filters on a general spot.



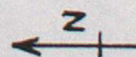


Figure  
2

AVHRR  
Channel 2  
(vis)

Line of cross-section X











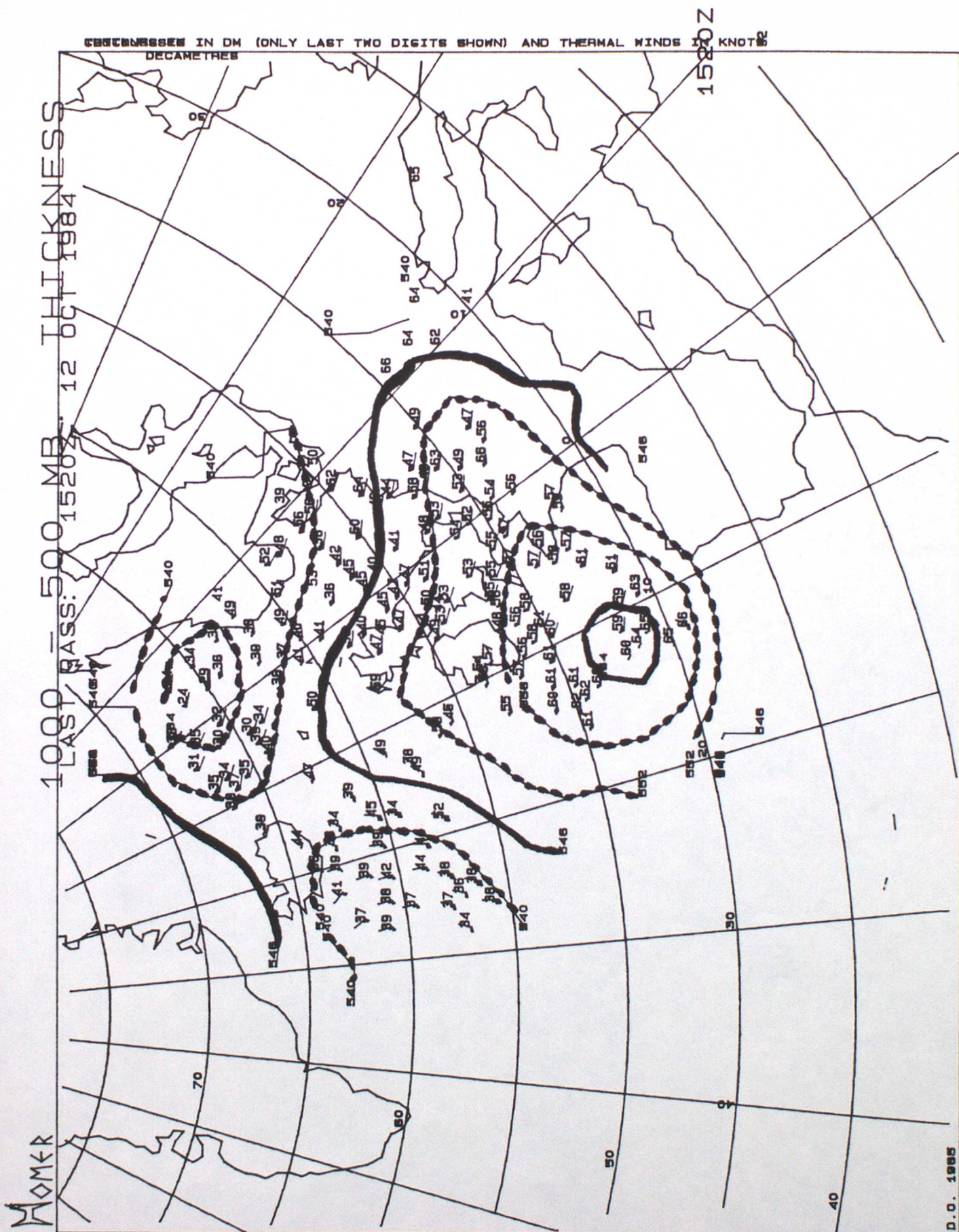


Figure 5 1000-500mb Thickness contoured. Current LASS system.



# LAST-PASS PLTRET

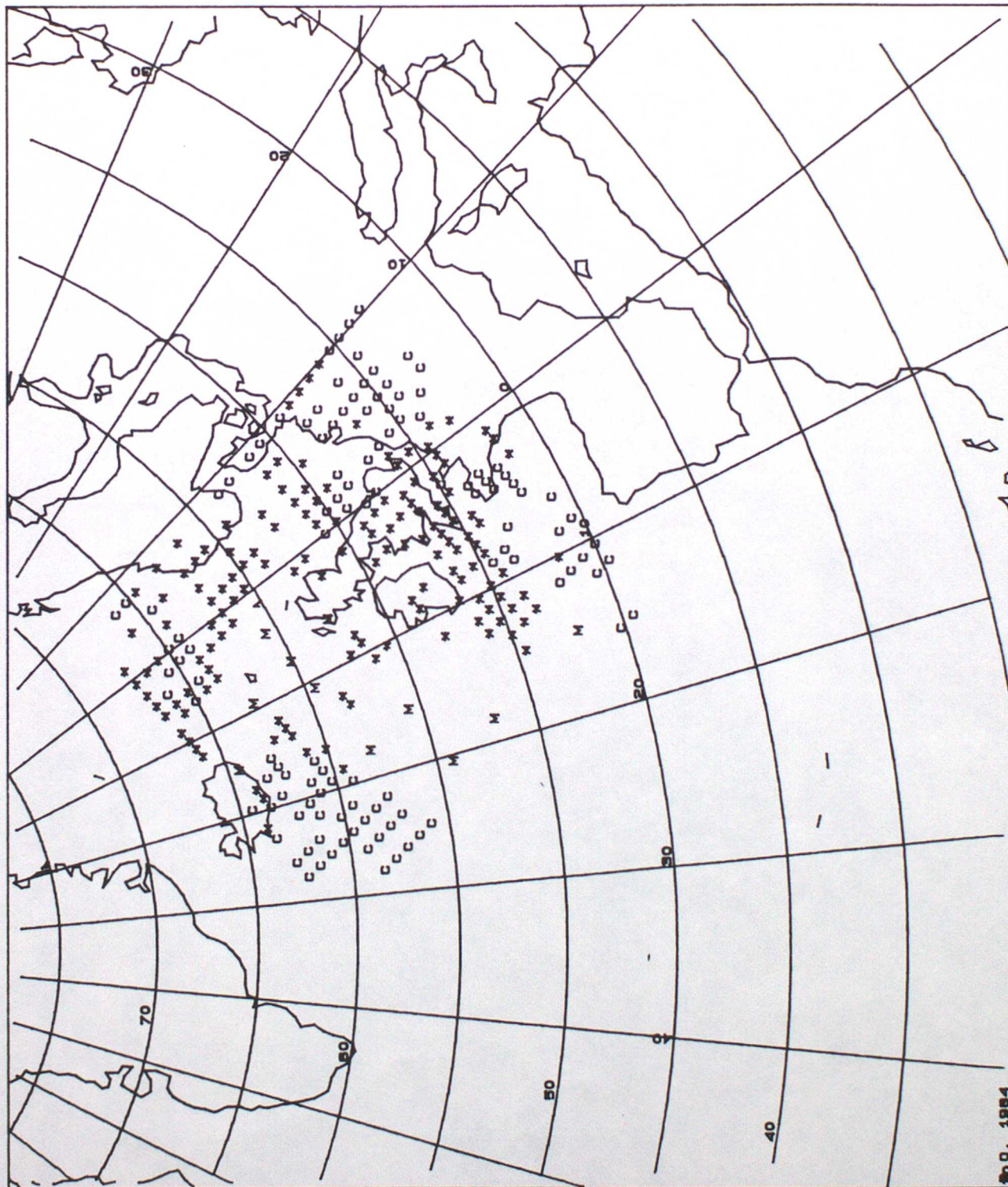
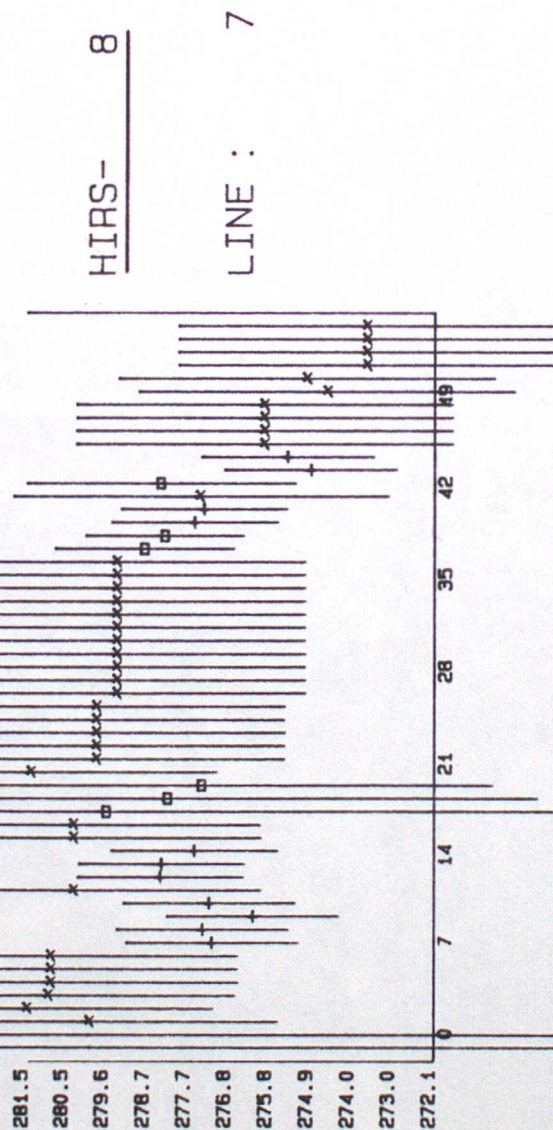


Figure 6  
LASS: Route plan

C = 'clear'  
\* = N-Star  
M = MSU-only



# Brightness Temperature



+ CLEAR  
 \* REGRESSION  
 φ N-STAR

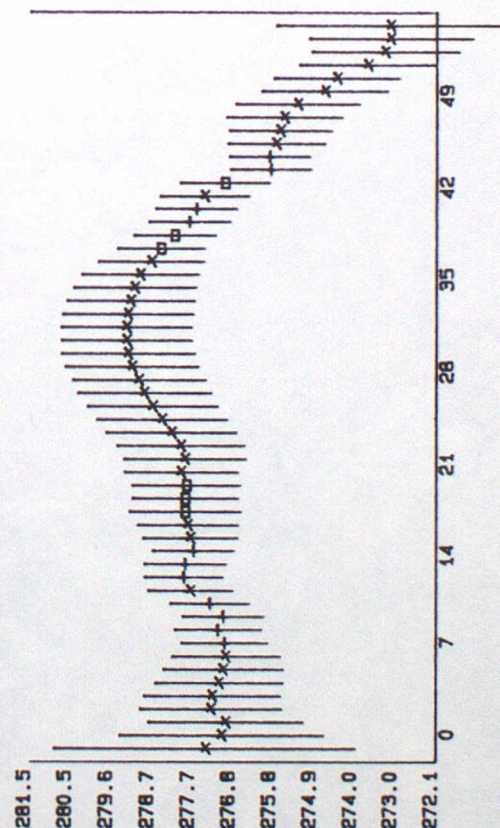


Figure 7  
 Brightness temperature  
 Cross-section



# HIRS-MSU Bias

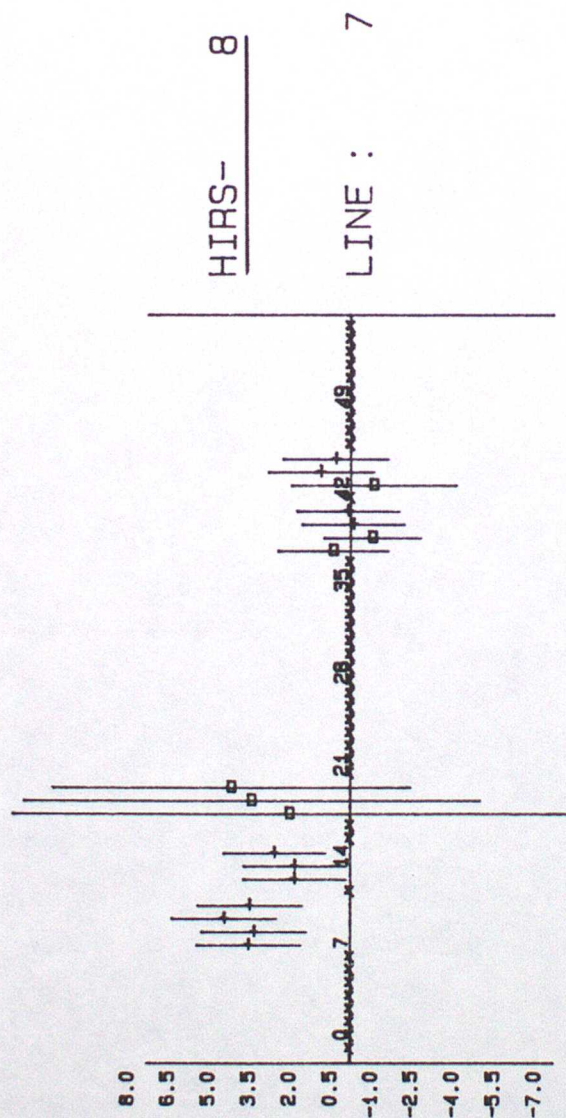


Figure 8  
Bias Cross-section

+ CLEAR  
\* REGRESSION  
Φ N-STAR

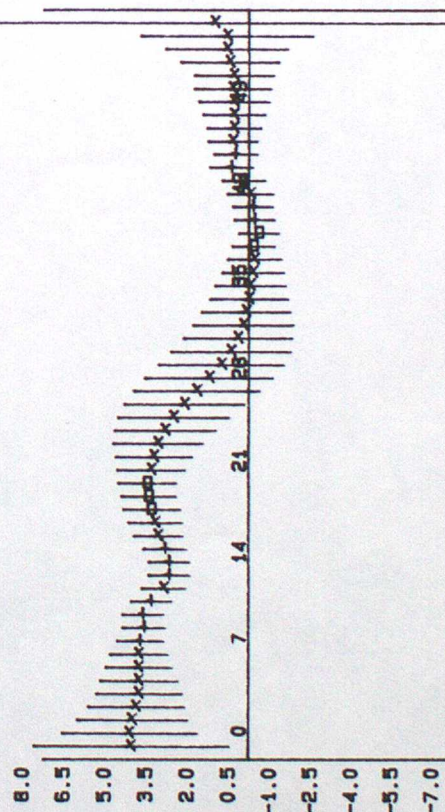




Figure A1 The N\* method and its error sources

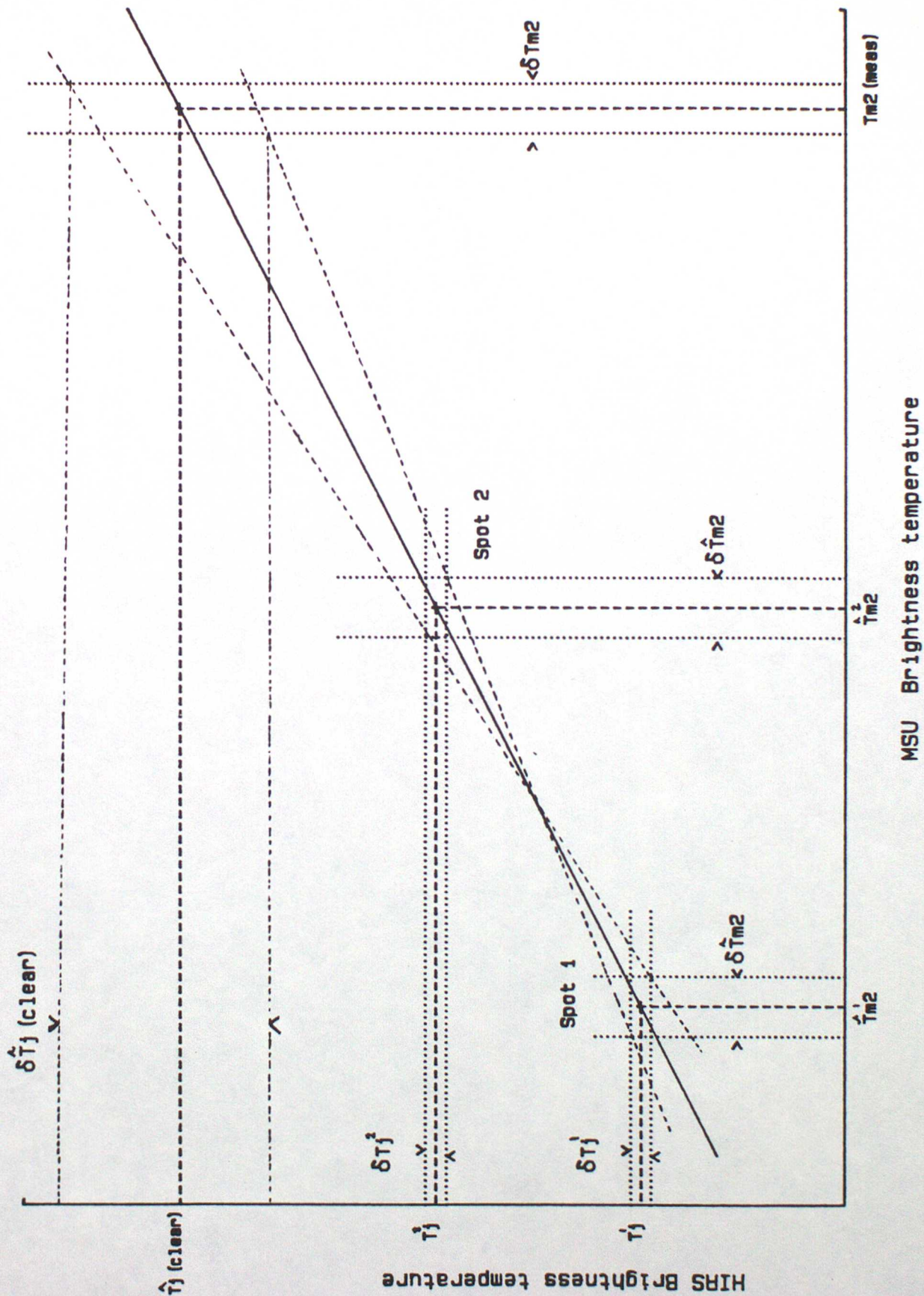




Figure B1

				$\lambda^4$				
			$2\lambda^4 \dashrightarrow$	$\lambda^3$	$2\lambda^4$			
		$3\lambda^4$	$2\lambda^3 \leftarrow$	$\lambda^2 + 2\lambda^4$	$\lambda^3$	$\lambda^4$		
	$\lambda^4$	$\lambda^3$	$\lambda^4 + \lambda^2 \dashrightarrow$	$\lambda + \lambda^3$	$\lambda^2 + \lambda^4$	$\lambda^3$	$\lambda^4$	
$\lambda^4$	$\lambda^3$	$\lambda^2$	$\lambda \leftarrow$	(2)	$\lambda \rightarrow$	$\lambda^2$	$\lambda^3$	$\lambda^4$
	$\lambda^4$	$\lambda^3$	$\lambda^2 + \lambda^4$	$\lambda + \lambda^3 \leftarrow$	$\lambda^2 + \lambda^4$	$\lambda^3$	$\lambda^4$	
		$\lambda^4$	$\lambda^3$	$\lambda^2 + 2\lambda^4 \rightarrow$	$2\lambda^3$	$3\lambda^4$		
			$\lambda^4$	$\lambda^3 \leftarrow$	$2\lambda^4$			
				$\lambda^4$				

Shows the contribution of a centre spot, in terms of powers of  $\lambda$ , to its surrounding spots. The weight given to itself is 2, because of the two filter system.

For clarity, only terms of  $\lambda$  up to power 4 are shown.



Figure B2 1) - 6)

Cross-section of weights with a  $1-\lambda$  system

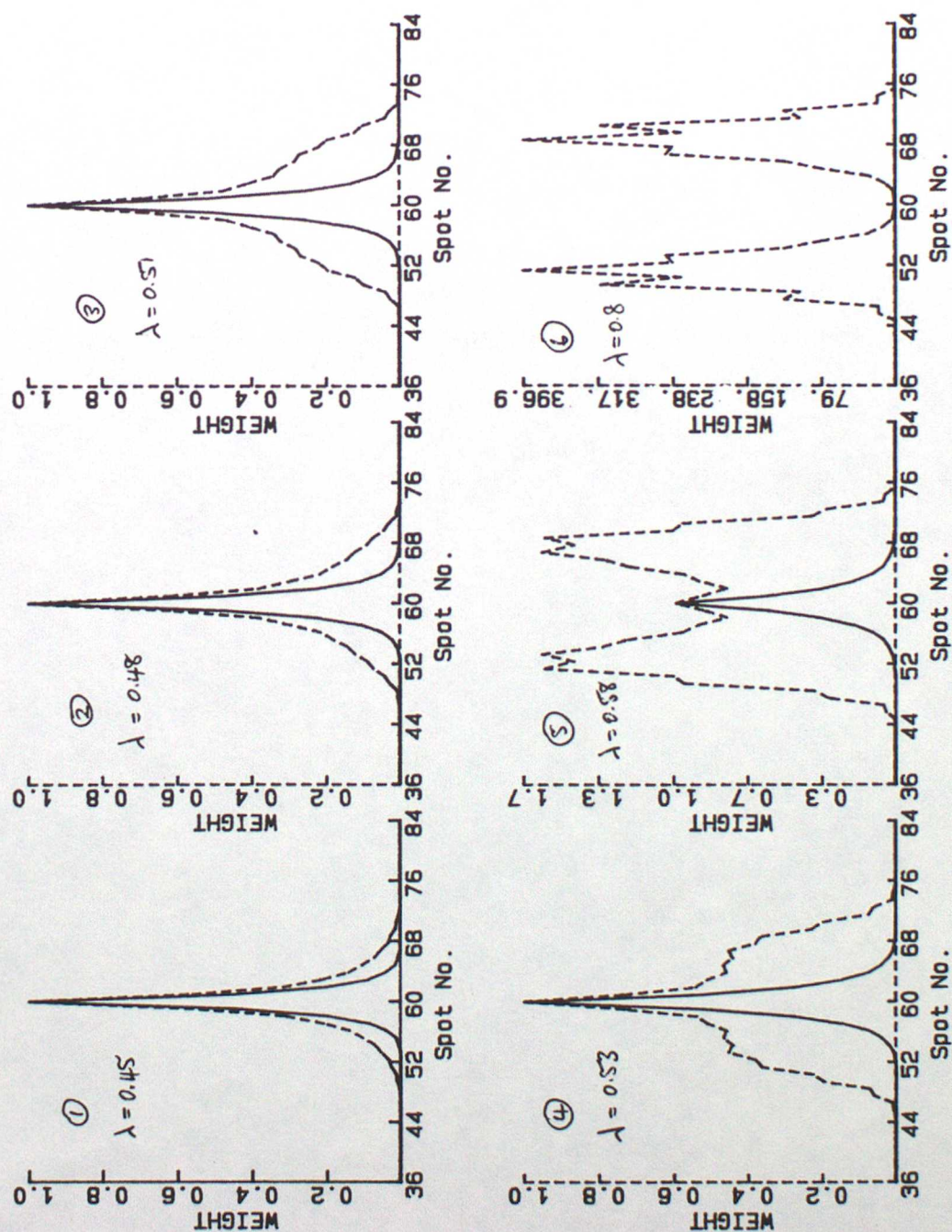
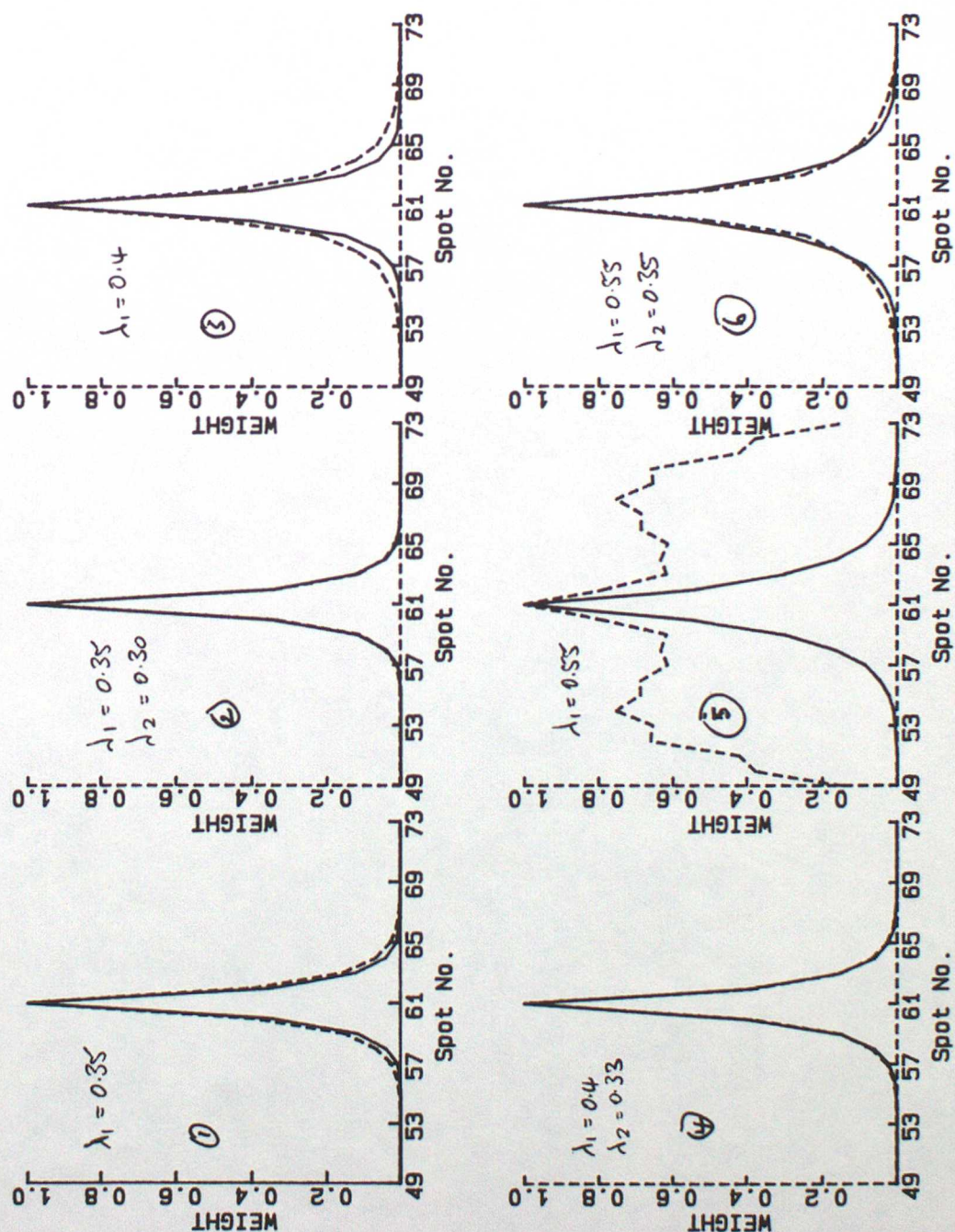


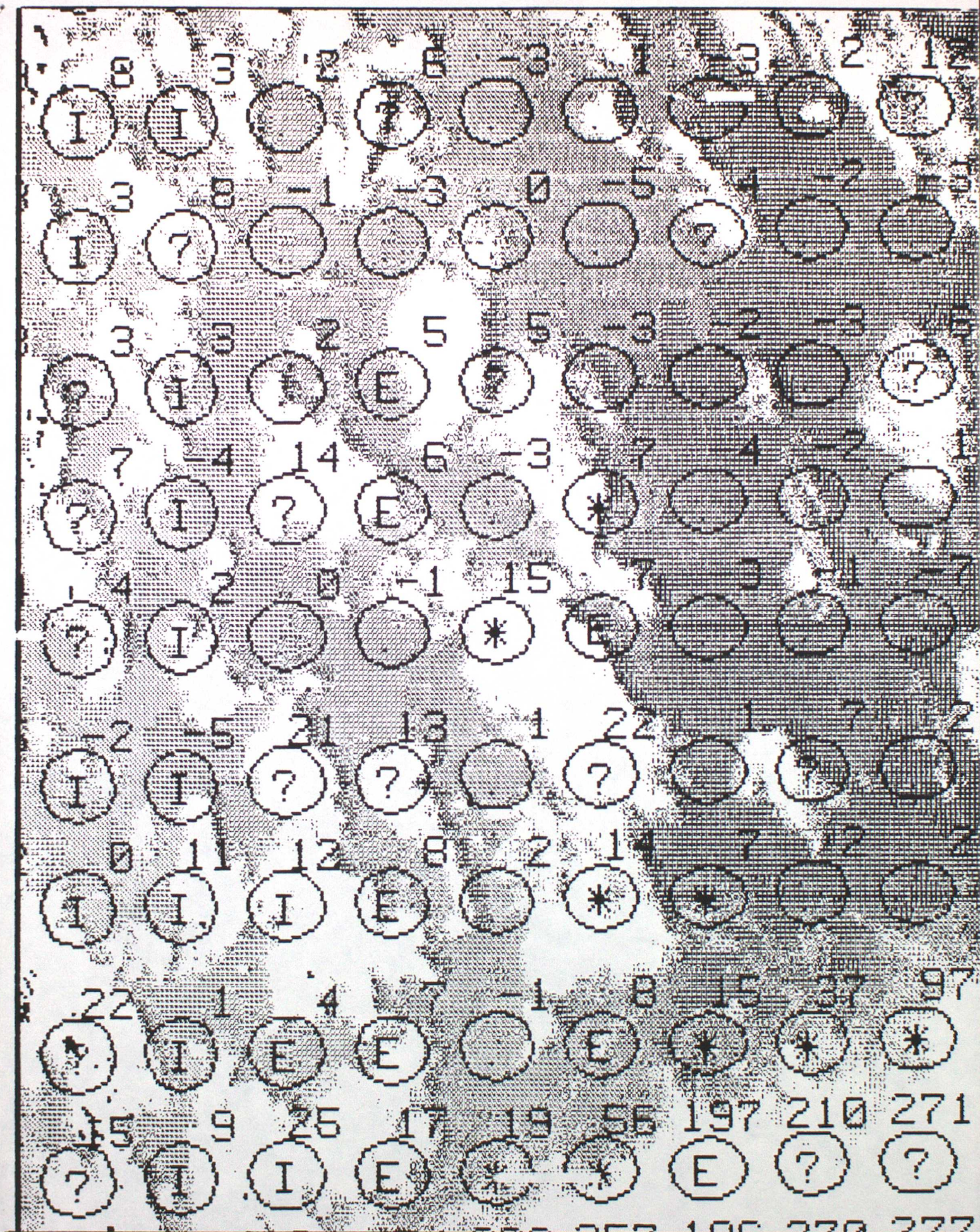


Figure B3 1) - 6)

Cross-section of weights with 2- $\lambda$  system



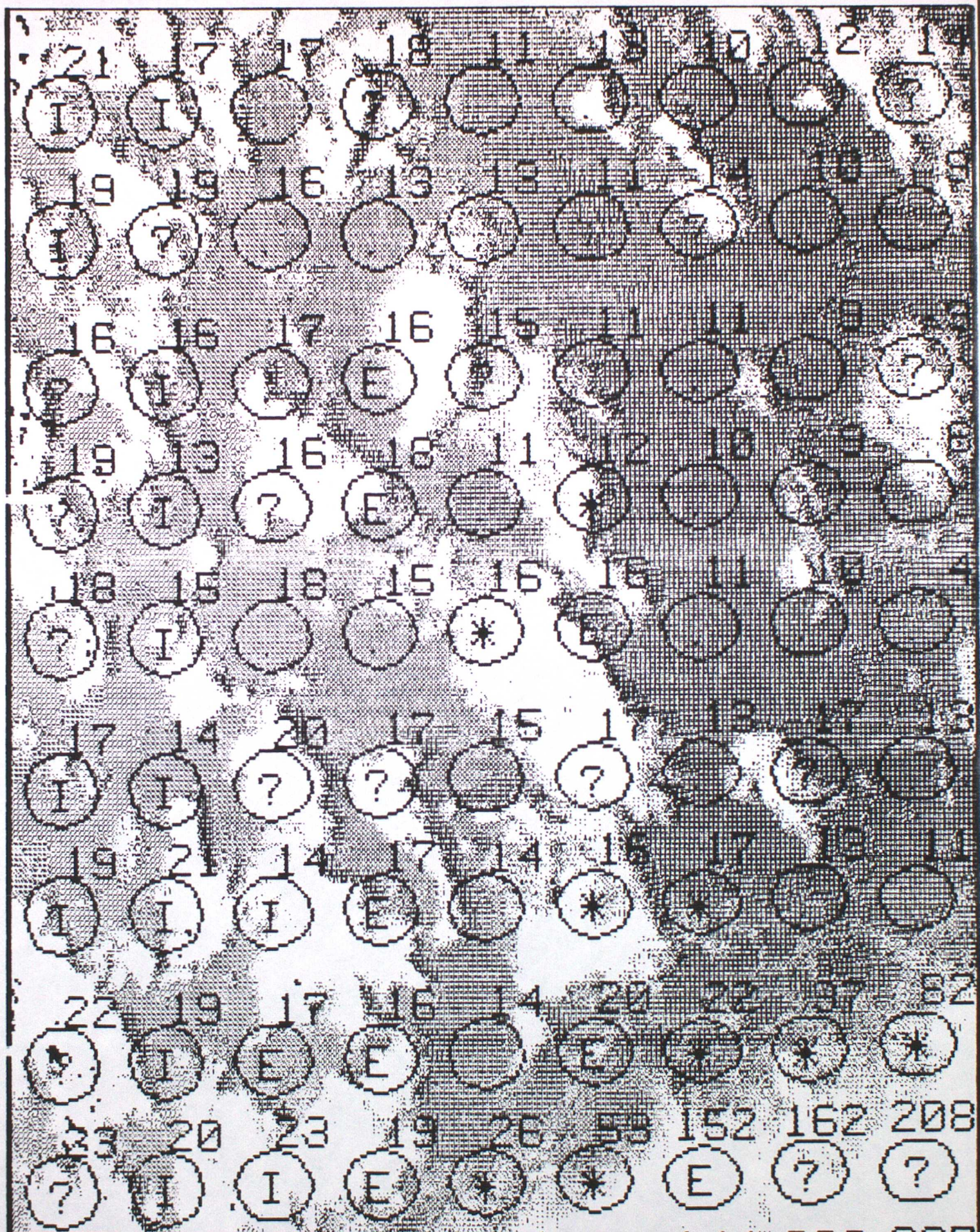




HIRS on AVHRR : 10 OCT 1984 : LASC Longwave .  $T_{M2} - \hat{T}_{M2}$  (deg $\times 10$ )

Figure E1

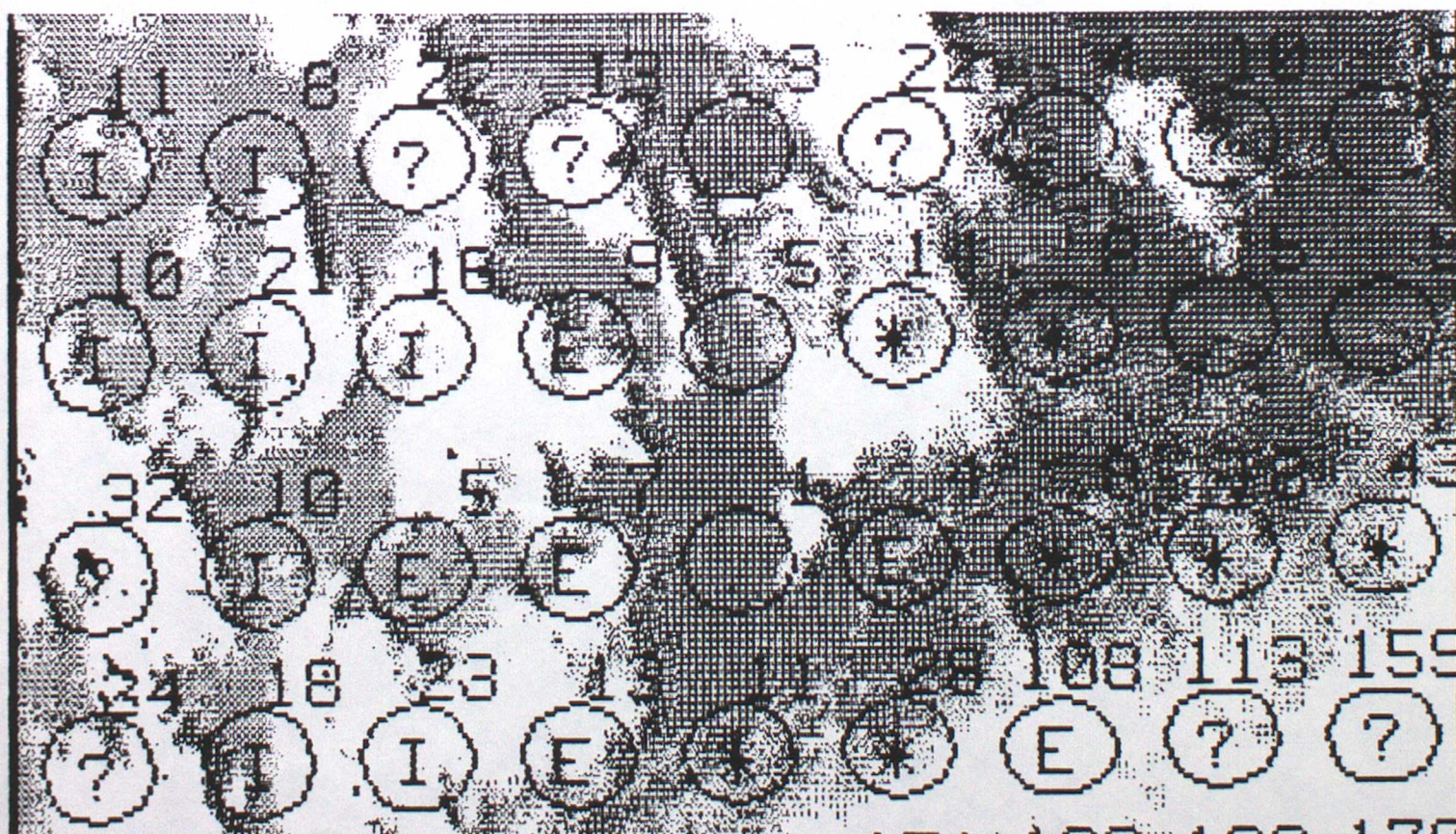
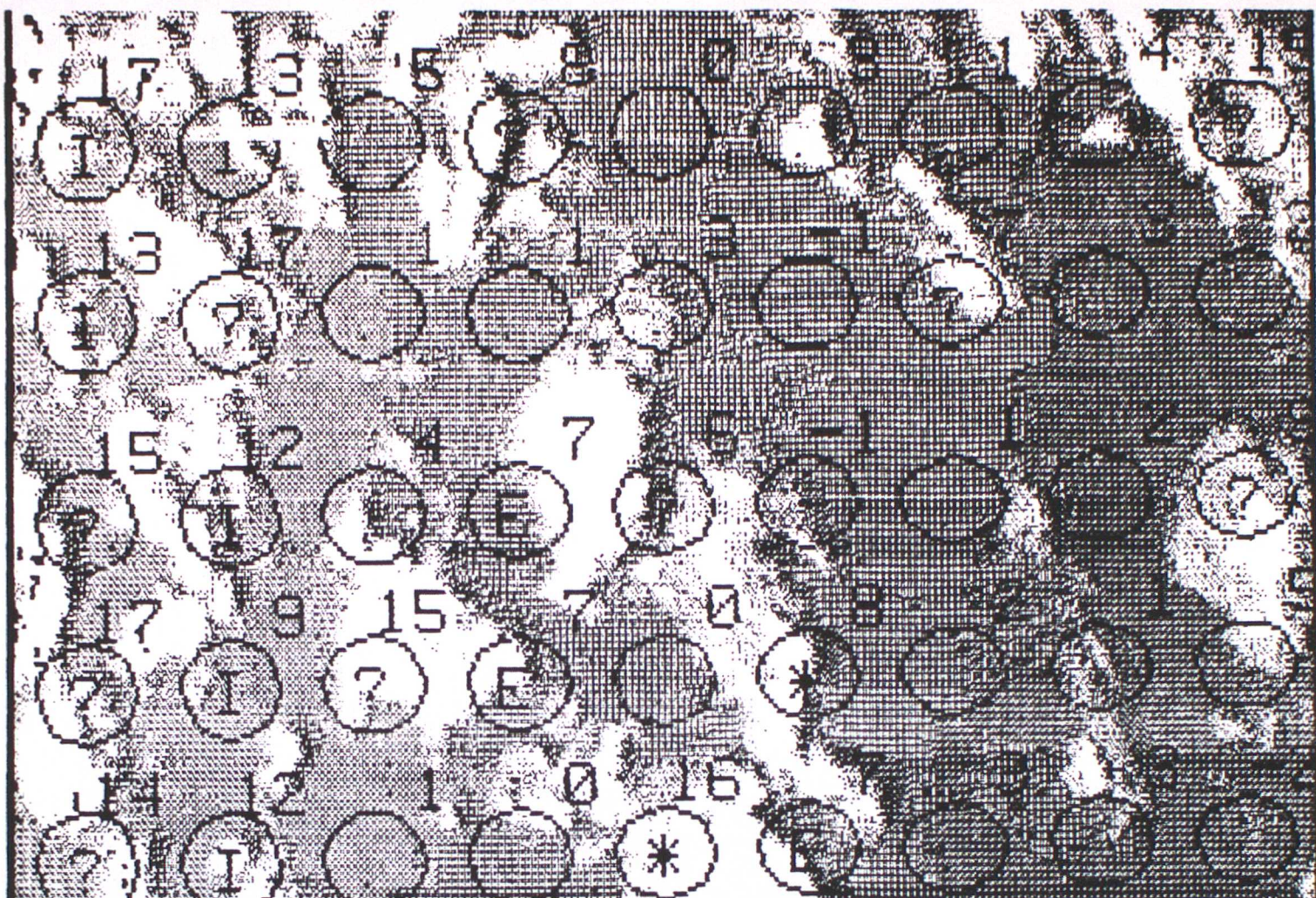




HIRS on AVHRR : 10 OCT 1984 : NESDIS Longwave  $T_{H2} - \hat{T}_{H2}$  (deg x 10)

Figure E2

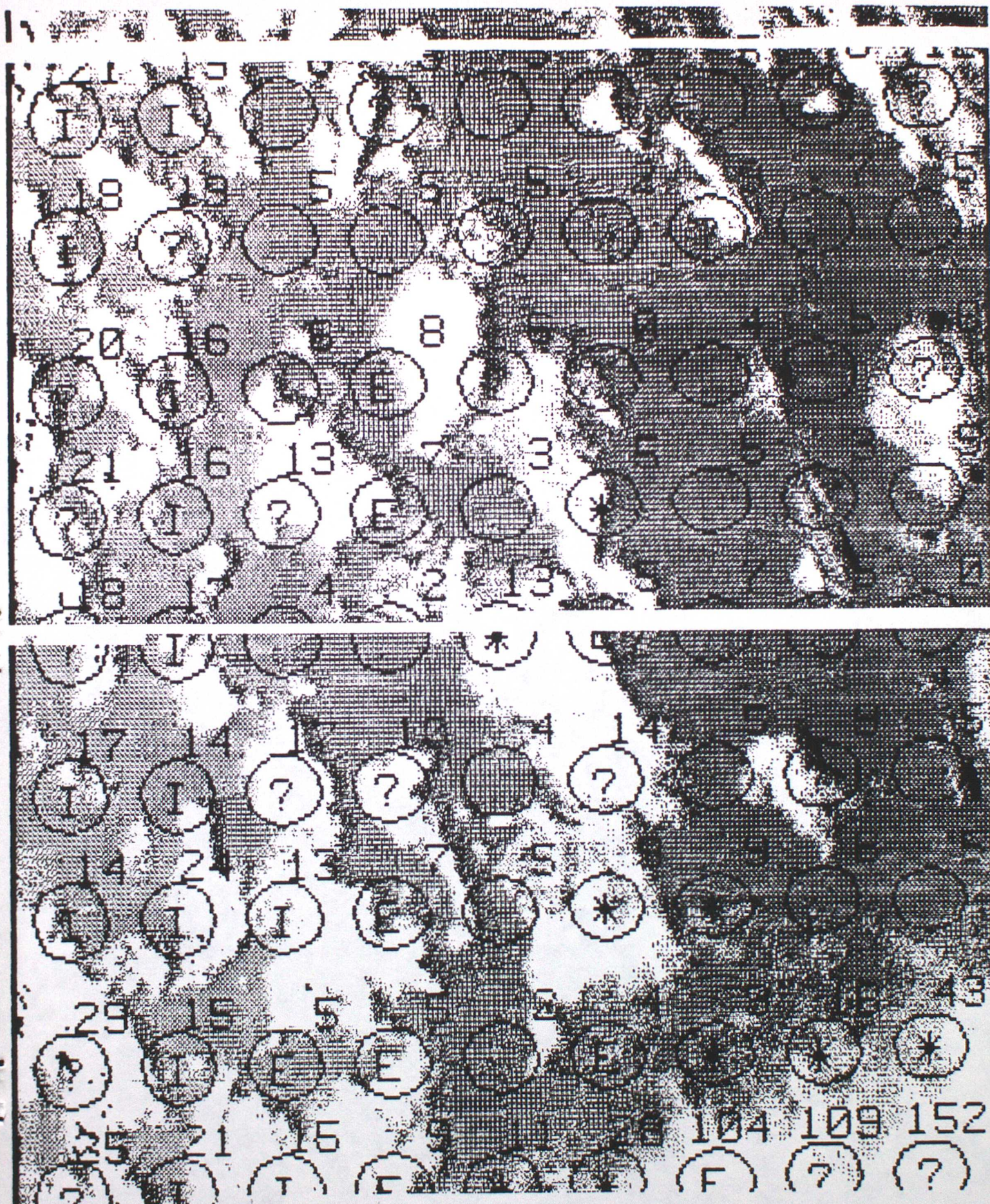




HIRS on AVHRR : 10 OCT 1984 : LASC Shortwave Tm2- $\hat{T}m2$  (Deg $\times 10$ )

Figure E3

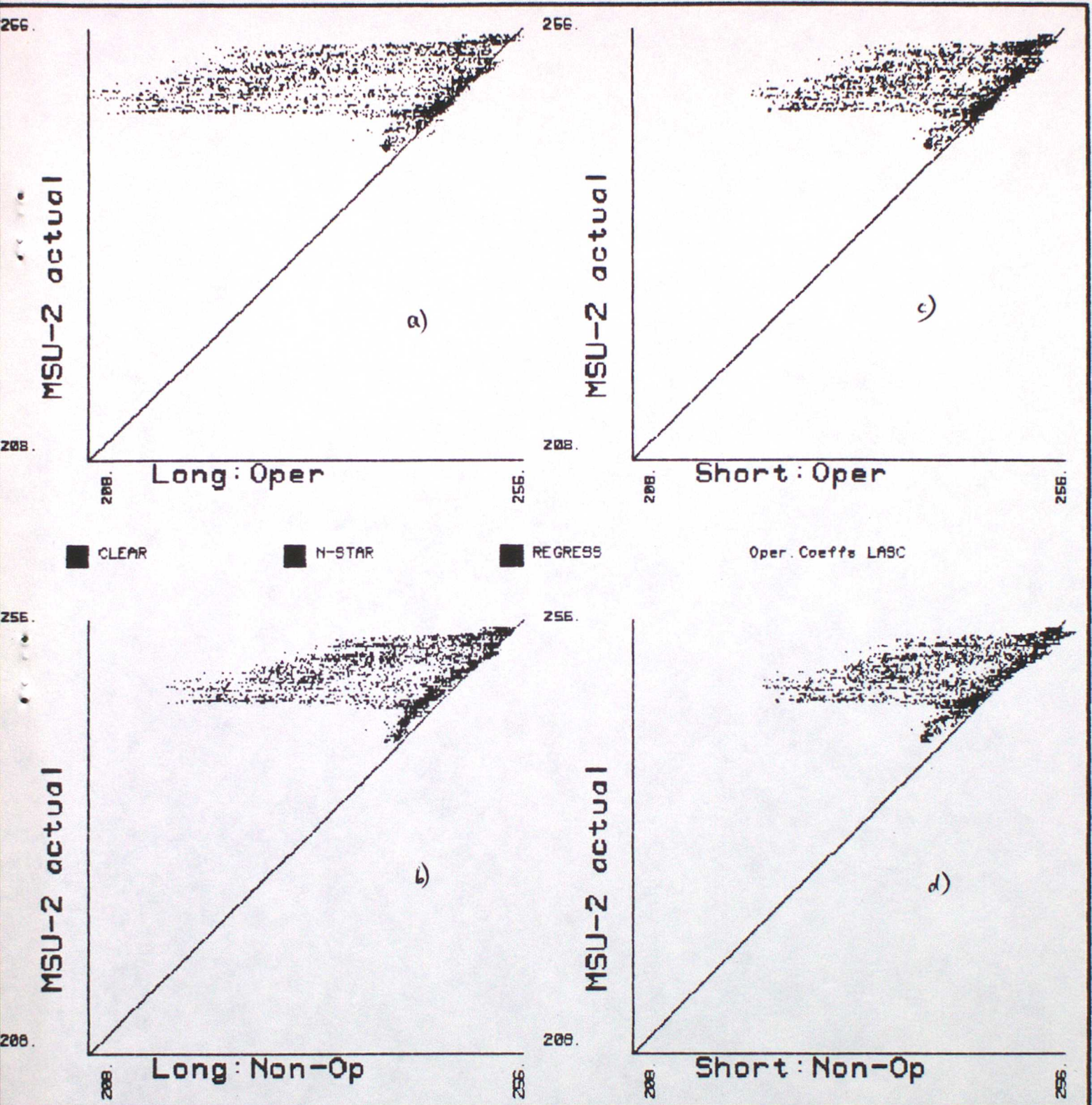




HIRS on AVHRR : 10 OCT 1984 : NESDIS Shortwave  $T_{m2} - \hat{T}_{m2}$  (DEG $\times 10$ )

Figure E4





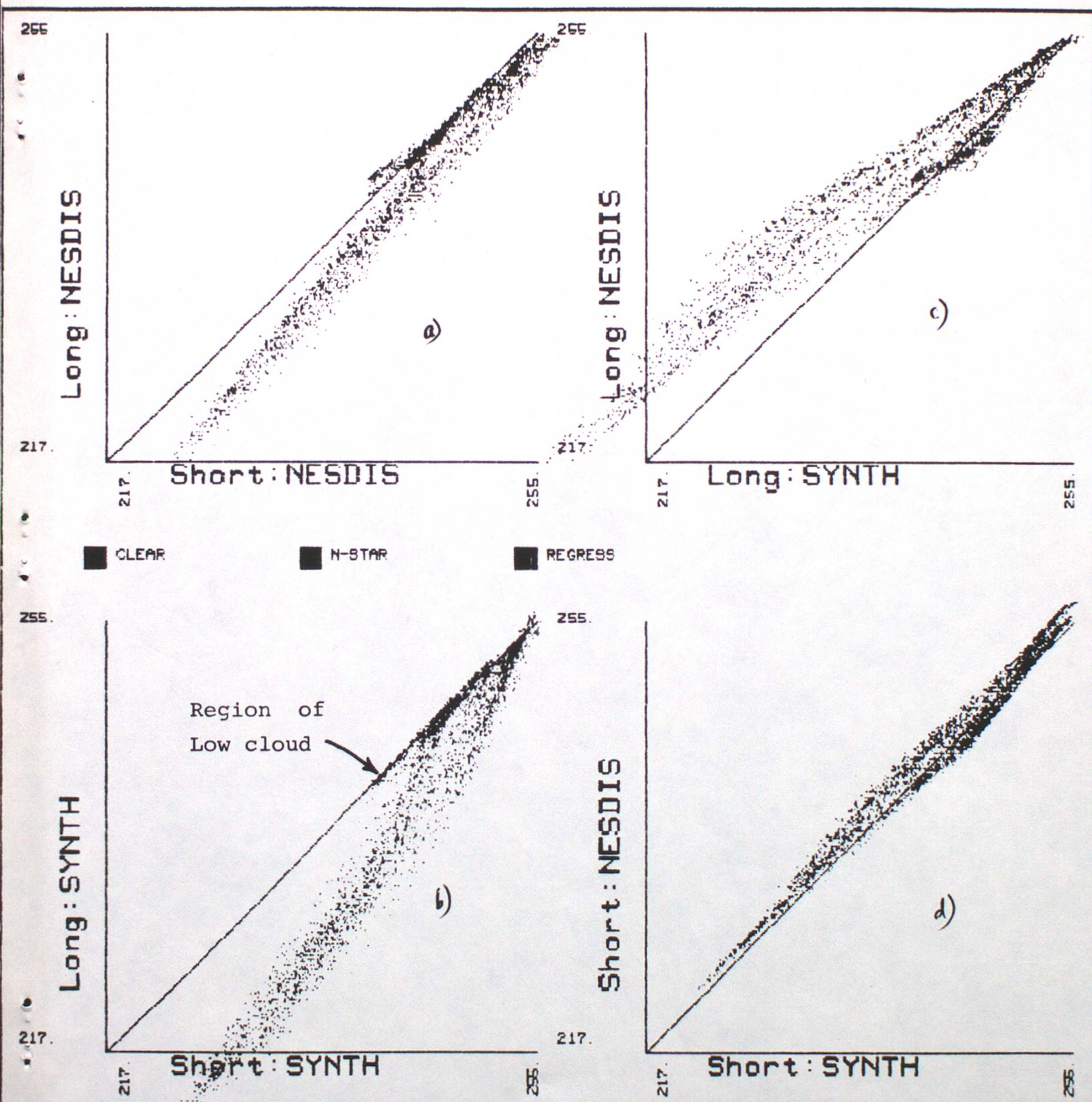
ARGS screen dump taken at 18:13:49 27-DEC-84

Figures ES a) → d)

MSU-2 Scatter plots



120CT MS PLOT 27-DEC-84 10:34Z



ARGS screen dump taken at 10:35:08 27-DEC-84

Figures E6 a) → d)  
MSU-2 Scatter plots